Draft version August 23, 2024
Typeset using LaTeX **twocolumn** style in AASTeX63

Ages of Stars and Planets in the Kepler Field Over the First Four Billion Years

Luke G. Bouma,[1,*] Lynne A. Hillenbrand,[1] Andrew W. Howard,[1] Howard Isaacson,[2] Kento Masuda,[3] and Elsa K. Palumbo[1,4]

[1]*Department of Astronomy, MC 249-17, California Institute of Technology, Pasadena, CA 91125, USA*
[2]*Astronomy Department, University of California, Berkeley, CA 94720, USA*
[3]*Department of Earth and Space Science, Osaka University, Osaka 560-0043, Japan*
[4]*Department of Statistics & Data Science, Carnegie Mellon University, Pittsburgh, PA 15213, USA*

(Received 2024 June 21; Revised —; Accepted —)

ABSTRACT

Recent analyses of FGK stars in open clusters have helped clarify the precision with which a star's rotation rate and lithium content can be used as empirical indicators for its age. Here we apply this knowledge to stars observed by Kepler. Rotation periods are drawn from previous work; lithium is measured from new and archival Keck/HIRES spectra. We report rotation-based ages for 23,813 stars (harboring 795 known planets) for which our method is applicable. We find that our rotational ages accurately recover the ages of stars in open clusters spanning 0.04-2.5 Gyr; they also agree with $\gtrsim$90% of the independent lithium ages. The resulting yield includes 63 planets younger than 1 Gyr at 2σ, and 109 with median ages below 1 Gyr. This is about half the number expected under the classic assumption of a uniform star formation history. We find that the scarcity of sub-gigayear systems can be attributed to the star formation rate in the Kepler field smoothly decreasing by a factor of 2.81 ± 0.12 over the past 3 Gyr. We observe this trend both in known planet hosts and in the parent stellar sample. This "demographic cliff" in the Galaxy's star formation history has been previously reported, and its confirmation helps clarify the age distribution of the known transiting exoplanets.

Keywords: Stellar ages (1581), Planet hosting stars (1242), Field stars (2103), Exoplanet evolution (491), Milky Way evolution (1052)

1. INTRODUCTION

Exoplanet science is thriving, fueled by the discovery of thousands of worlds orbiting close to their host stars (Borucki et al. 2010; Ricker et al. 2015). However, most known exoplanets are billions of years old. This fact leaves many gaps in our knowledge of the exact physical and dynamical origins of these objects. The reason is that processes such as thermal cooling (Fortney et al. 2007), atmospheric loss (Owen 2019), giant impacts (Raymond et al. 2014), and dynamical instabilities (Izidoro et al. 2017) are expected to be most efficient over timescales of much less than 1 Gyr. For most known exoplanets, these processes have run their course.

Young (<1 Gyr) exoplanets represent one means of building the timeline for exoplanet evolution. Informative individual exemplars include HIP 67522b, a Jupiter-sized planet with a sub-Neptunian mass (Rizzuto et al. 2020; Thao et al. submitted), and V1298 Tau, a resonant chain of puffy planets that is a likely precusor to the compact multiplanet systems (David et al. 2019). Population-level analyses have similarly suggested differences in the size distribution of young exoplanets relative to their older counterparts (Berger et al. 2020a; David et al. 2021; Sandoval et al. 2021; Christiansen et al. 2023; Vach et al. 2024).

Discovering a young planet requires solving two problems: finding the planet and measuring the star's age. Each problem admits a range of solutions (e.g. Marois et al. 2008; Quinn et al. 2012; Tran et al. 2024). In this article we will consider planets whose existence has been previously established using transits, and infer new stellar ages using rotation and lithium.

To begin, imagine that the ages of nearby stars in the Galaxy are uniformly distributed from 0–10 Gyr (Binney et al. 2000; Nordström et al. 2004). This approximation suggests that $\approx$1% of nearby stars have $t<100$ Myr, and $\approx$10% have $t<1$ Gyr. Studies of currently forming protoplanets (Keppler et al. 2018), and of exoplanets evolving just after disk dispersal (e.g. Klein et al. 2022), are thereby capped in their maximum achievable sample sizes by the tyranny of the galactic star formation rate.

Despite this and other observational challenges, young close-in planet discovery has matured over the past decade, primarily due to Kepler, K2, TESS, and Gaia (e.g. Mei-

Corresponding author: Luke G. Bouma
bouma.luke@gmail.com

* 51 Pegasi b Fellow

bom et al. 2013; Mann et al. 2016; Curtis et al. 2018; Livingston et al. 2018; David et al. 2019; Bouma et al. 2020; Rizzuto et al. 2020; Plavchan et al. 2020; Newton et al. 2021; Nardiello et al. 2022; Barber et al. 2022; Zhou et al. 2022; Zakhozhay et al. 2022; Wood et al. 2023). The strategy pursued by most groups during the 2010s was to focus on stars with known ages—obvious members of open clusters—and to search them for transiting planets. The resulting stellar, and assumed planetary, ages are precise at the ≈10% level. An alternative strategy, facilitated by Gaia, is to select transiting planets based on empirical youth indicators, and to then search their local neighborhoods for comoving companions (e.g. Tofflemire et al. 2021).

While stellar ensembles provide the gold standard for astronomical ages, this "cluster-first" approach has a major limitation: most stars are in the field. Only $\lesssim$1% of stars within ≈500 pc have been associated with their birth cluster (e.g. Zari et al. 2018; Cantat-Gaudin et al. 2020; Kounkel et al. 2020; Kerr et al. 2021). The implication for known planetary ages can appreciated by querying the NASA Exoplanet Archive (NEA; Akeson et al. 2013) for transiting planets younger than 1 Gyr. Requiring $t<1$ Gyr at 2σ precision gives ≈50 such planets at the time of writing. Most of these young planets are in clusters, and were found by Kepler, K2, or TESS. However, these surveys have cumulatively discovered ≈5,000 planets. Assuming a constant star formation history, we would expect an order of magnitude more sub-gigayear transiting planets than the 50 currently known.

This study aims to resolve two questions. First, how wrong is it to assume a uniform age distribution for transiting planet host stars? Second, where are the missing young planets? We will find that uniform is wrong by a factor of a few, and that stellar activity may be a less significant bias in young transiting planet detection than the challenge of precisely determining ages for field stars.

Despite Kepler's main mission ending quite some time ago, the ages of many Kepler planets remain uncertain. While isochrone ages have been calculated for Kepler stars (Berger et al. 2020a) and Kepler Objects of Interest (KOIs; Petigura et al. 2022), such ages are most precise for stars whose luminosities and temperatures separate them from the main sequence. For sub-gigayear stars on the main sequence, isochrone ages are therefore limited.

Stellar rotation periods offer a promising alternative. The idea of using a star's spin-down as a clock has a rich history (Skumanich 1972; Noyes et al. 1984; Kawaler 1989; Barnes 2003; Mamajek & Hillenbrand 2008; Angus et al. 2015). Empirical models now yield ages precise to $\lesssim$30% for FGK stars between 1-4 Gyr, and constraining age posteriors for younger ages (Bouma et al. 2023). Physics-based models (Matt et al. 2015; Gallet & Bouvier 2015; Spada & Lanzafame 2020) can connect these empirical relations to the evolution of stellar winds, internal structure, and angular momentum transport.

Rotation-based ages have been reported for various subsets of Kepler stars since the early data releases (e.g. Walkowicz & Basri 2013; McQuillan et al. 2014; Reinhold & Gizon 2015; Angus et al. 2018). More recent work has further explored incorporating information from stellar kinematics (Lu et al. 2021, 2024), and from stellar colors, luminosities, and starspot amplitudes (Mathur et al. 2023). Our analysis is motivated by a few factors that can yield improvements, particularly for sub-gigayear stars. These factors are as follows.

i) The Kepler Object of Interest catalog, and our vetting of false positives within it, has now reached maturity (e.g. Thompson et al. 2018).

ii) Measured rotation periods of FGK stars in open clusters now show not only the average evolution of $P_{\rm rot}(T_{\rm eff}, t)$, but also how the astrophysical dispersion of stars around this average converges by the ≈700 Myr age of Praesepe (e.g. Curtis et al. 2019; Gillen et al. 2020; Rampalli et al. 2021; Fritzewski et al. 2021; Rebull et al. 2022; Dungee et al. 2022; Boyle & Bouma 2023).

iii) Using open cluster data, we can marginalize over the range of ages that might explain any one star's rotation period (Bouma et al. 2023). This represents an improvement in the accuracy of uncertainty propagation relative to previous calibrations.

iv) We can identify binary stars with greater fidelity than in the past, which can clarify otherwise problematic estimates of rotation-based ages.

v) New open clusters in various stages of dissolution have been found in the Kepler field (e.g. Kounkel & Covey 2019; Kerr et al. 2021; Barber et al. 2022). These clusters offer stars that we can use to test the reliability of the available single-star age-dating methods.

Recent years have also yielded improvements in the lithium age scale. Lithium ages include depletion boundary ages for M dwarfs and brown dwarfs in star clusters, and decline-based ages for individual field FGK stars (Soderblom 2010). The latter approach relies on the observed decrease of Li abundances in partially-convective stars as they age (e.g. Sestito & Randich 2005). The theoretical explanation for these observations is debated (e.g. Chaboyer et al. 1995; Denissenkov et al. 2010; Carlos et al. 2019). Empirical understanding however has improved due to work by Jeffries et al. (2023), who modeled the time evolution of the Li I 6708 Å equivalent width (EW) using a set of 6,200 stars in 52 open clusters. Two-sided lithium ages are useful for Kepler (FGK) stars between ≈0.03-0.5 Gyr, though with a strong dependence on spectral type. The precision of lithium ages in this regime are now in the range of 0.3-0.5 dex.

We discuss our method for selecting the star and planet samples in Section 2, and describe the origin of our adopted stellar parameters other than ages in Section 3. We describe our age-dating methods in Sections 4 and 5, and test them in Section 6 using clusters in the Kepler field. We discuss population-level trends in Sections 7 and 8, and offer a few conclusions in Section 9.

2. SELECTING THE STARS AND PLANETS

This work is focused on Kepler stars for which ages can be inferred using either rotation, lithium, or both. Such

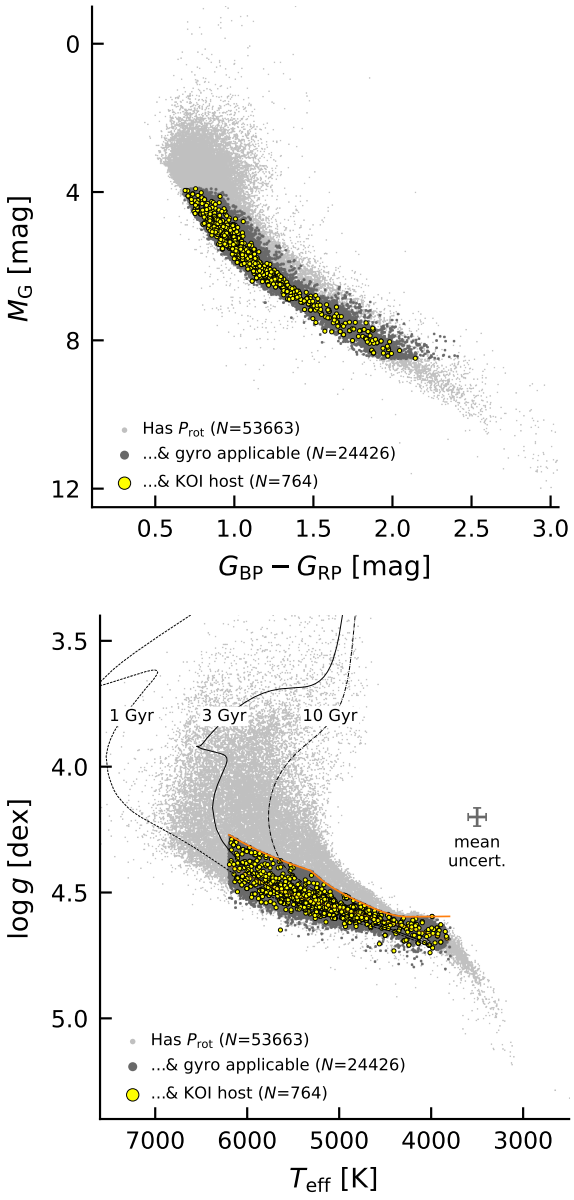

Figure 1. The stars. Our analysis focuses on stars observed by Kepler with previously reported rotation periods (gray points). The rotation periods are primarily drawn from Santos et al. (2019, 2021). About half of the stars with rotation periods are suitable for gyrochronology (dark gray points), based on factors including their non-binarity and proximity to the main sequence (orange line in lower panel; see Section 4.1). Some host "confirmed" or "candidate" KOIs that meet additional planetary quality criteria (yellow points; Section 4.2). Surface gravities and effective temperatures were derived photometrically by Berger et al. (2020b). Isochrones in the lower panel are from MIST (Choi et al. 2016).

stars are a minority of the ≈160,000 Kepler targets. Rotation periods have been reported for roughly one in three Kepler targets (e.g. McQuillan et al. 2014; Santos et al. 2021). High-resolution spectra suitable for measurement of the Li I 6708 Å doublet have only been acquired for the Kepler objects of interest (KOIs), which comprise a few percent of Kepler's targets. In the following, we will describe the set of stars that we adopt with measured rotation periods (Section 2.1), the set of objects we adopt as hosting planets (Section 2.2), and the subset of these with high-resolution spectra suitable for lithium analysis (Section 2.3). Figure 1 provides a visualization of the various samples.

2.1. *Stellar Rotation Periods*

To select stars with rotation periods, we turn to previous work. Many investigators have derived rotation periods both specifically for KOIs (McQuillan et al. 2013; Walkowicz & Basri 2013; Mazeh et al. 2015; Angus et al. 2018; David et al. 2021), and also for the broader set of all Kepler target stars (McQuillan et al. 2014; Reinhold & Gizon 2015; Santos et al. 2019, 2021; Reinhold et al. 2023). These studies used a range of detection methods and selection functions. We are interested in understanding the age distribution of all Kepler target stars irrespective of KOI status. Out of these studies, the most homogeneous analyses of both Kepler targets and KOIs appear to be those by Santos et al. (2019, 2021), hereafter S19 and S21. For a discussion of the work by Reinhold et al. (2023), please see Appendix A. S19 and S21 combined a wavelet analysis and autocorrelation-based approach, and cumulatively reported rotation periods for 55,232 main-sequence and subgiant FGKM stars. They included known KOIs and binaries in their analysis, and removed transits and eclipses during the stellar rotation measurement process.

We therefore adopt the results of S19 and S21 as our default rotation periods. S21 provided a comparison against McQuillan et al. (2014) (hereafter M14); the brief summary is that the periods agree for 99.0% of the 31,038 period detections in common between the two studies. S21 classified the 2,992 remaining stars from M14 as not showing rotation periods based on updated knowledge of contaminants (e.g. giant stars and eclipsing binaries) and visual inspection. In addition, S21 reported rotation periods for 24,182 main-sequence and subgiant FGKM stars that were not reported as periodic by M14. Many of these reported detections have lower variability amplitudes and longer periods than those reported by M14.

Analyzing the compilation of S19 and S21 rotation periods for the KOI hosts, we noticed that some known KOIs with rotation periods were missing. This is not surprising, since the rotation periods of KOIs have received more scrutiny than those of ordinary Kepler stars. We therefore decided to split our subsequent analysis into a homogeneous portion that used only the S19 and S21 data, and an inhomogeneous portion that also considered a broader set of available KOI rotation periods. For the latter portion, we first included 32 KOIs with orbital and rotation periods within ≈20% that had been excluded from the S19 and S21 catalogs (A. Santos, private communication). We then incorporated an additional 178 rotation periods for KOI hosts that David et al. (2021) described as either "reliable" or "highly reliable" in their visual analysis of previously reported KOI rotation periods from McQuillan

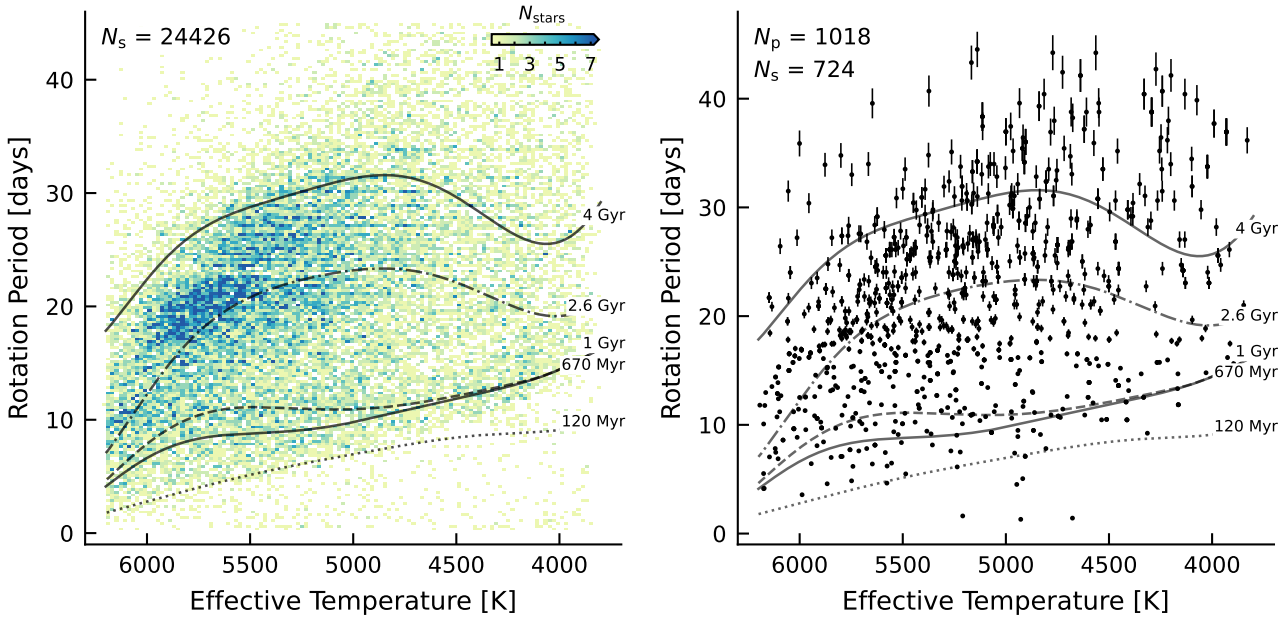

Figure 2. Rotation periods for Kepler target stars (left) and known planet hosts (right). The gray lines are seventh-order polynomials fitted to the slow rotation sequences of open clusters (see Section 3.3 of Bouma et al. 2023). The 2-D histogram of the stellar sample (left) includes only apparently single stars near the main sequence with $\log g > 4.2$, RUWE$<$1.4, and temperatures of 3800–6200 K. The planet-hosts (right) require the same stellar cuts, and include only the confirmed and candidate planets described in Section 4.2. The number of stars N_s and planets N_p are noted in the relevant panels. A simple estimate for the number of young planets discovered by Kepler follows by counting points below the rotational isochrones.

et al. (2013), Walkowicz & Basri (2013), Mazeh et al. (2015) and Angus et al. (2018). Inclusion of these additional KOI rotation periods is a supplementary measure aimed at completeness in our final KOI age catalog; the provenances of the individual adopted periods are noted in the relevant tables.

Finally, since our scope is focused on rotation-based ages, we restricted our attention to stars with reported $P_{rot}<45$ days. The slowest-rotating FGK stars in the open clusters used to calibrate our gyrochronology model have $P_{rot}\approx35$ days. Figure 2 shows a subset of the resulting 53,663 Kepler stars with rotation periods compiled from S19, S21, and our extended KOI list. The gray lines in this figure are the polynomials described by Bouma et al. (2023) that fit the slow rotation sequences of the Pleiades (Rebull et al. 2016), Praesepe (Rampalli et al. 2021), NGC-6811 (Curtis et al. 2019), NGC-6819 (Meibom et al. 2015), Ruprecht-147 (Curtis et al. 2020), and M67 (Barnes et al. 2016; Dungee et al. 2022; Gruner et al. 2023).

To assess the statistical uncertainties of our adopted rotation periods, we compared our periods with those reported by McQuillan et al. (2014). The details are in Appendix A. We found that for $P_{rot} \lesssim 15$ days, the two datasets agree at a precision of $\lesssim 0.01 P_{rot}$. At longer periods of $P_{rot} \approx 30$ days, the agreement was typically at the $\lesssim 0.03 P_{rot}$ level, and the envelope of the period difference increased roughly linearly with period. Based on this comparison, we adopted a simple prescription for the period uncertainties, such that there are 1% relative uncertainties below P_{rot} = 15 days, and a linear increase thereafter, with slope set to require 3% P_{rot} uncertainties at rotation periods of 30 days.

2.2. *Kepler Objects of Interest*

We considered planets in the NEA cumulative KOI table as of 2023 June 6, which included the best knowledge available on any given planet candidate while also incorporating human-based vetting. These planets represent a superset of those in the fully automated Q1-Q17 DR25 KOI Table (Thompson et al. 2018), which could be adopted in future work for planet occurrence rate calculations. This version of the cumulative KOI table included 4,716 objects that are either "confirmed" or "candidate" planets, after excluding known false positives.

2.3. *High Resolution Spectra*

The final piece of our analysis involves assessing ages based on the Li I 6708 Å doublet. We analyzed spectra from the High Resolution Echelle Spectrometer (HIRES; Vogt et al. 1994a) on the Keck I 10m telescope. These spectra were primarily collected through the California Kepler Survey (Petigura et al. 2017; Johnson et al. 2017; Fulton et al. 2017). We supplemented the existing archive with ≈10 hours of new observations for 22 stars between Fall 2022 and Spring 2024. These stars were chosen to ensure that confirmed planets with rotational evidence for ages below 1 Gyr had spectra, since this is the age range in which lithium is most likely to yield useful age constraints.

Lithium equivalent widths and abundances for the Kepler Objects of Interest were already analyzed by Berger et al. (2018) for roughly three quarters of the spectra in our sample. However, new spectra have since been acquired, and our approach and selection function are different. We therefore performed our own line width measurements on the reduced HIRES spectra.

We collected all blaze-corrected HIRES spectra from our group's observations of non-false positive Kepler Objects of Interest with a "multiple event statistic" (MES, *koi_max_mult_ev*) of at least 10. This yielded at least one spectrum for 1,464 stars hosting 2,174 planets. About half of these stars have measured rotation periods (797 stars and 1,170 planets, respectively). For stars with multiple spectra available, we analyzed only the spectrum with the highest number of counts. The resulting spectra were acquired between 2009 September 6 and 2024 May 16, and cumulatively comprise 304 hours of open-shutter time.

We measured the lithium equivalent widths using a procedure adapted from previous work (Bouma et al. 2021). Our stars of interest are FGK stars, and so the continuum in the vicinity of the Li I 6708 Å doublet is well-defined. We Doppler-corrected the spectra to a common reference wavelength by cross-correlating against a high S/N template for Kepler-1698, chosen because $|\gamma|<10\,\mathrm{km\,s^{-1}}$, $T_{\rm eff}\approx5000$ K and $v\sin i\approx5\,\mathrm{km\,s^{-1}}$, which puts it in the middle of our sample's temperature range and gives it mild line-broadening. We then trimmed the Doppler-corrected spectra to a local window centered on the lithium line, using a window width of 15 Å (we also considered 10 Å and 20 Å; the results were consistent). We continuum-normalized by fitting a third-degree Chebyshev series, while excluding regions with absorption lines. We then numerically integrated the resulting spectrum using a one-component Gaussian with free amplitude, width, and mean, and estimated uncertainties on the line width through a Monte Carlo procedure that bootstrapped against the local scatter in the continuum. The resulting EWs are shown in Figure 3.

Our EW measurement approach did not correct for the neighboring Fe I 6707.44 Å blend. To evaluate the accuracy and precision of our method, after applying an initial iteration on the 1,464 stars with spectra, we compared our lithium equivalent widths with those reported by Berger et al. (2018). For the stars in both samples, we found broad agreement at >30 mÅ, and significant differences at <30 mÅ because Berger et al. (2018) required positive EWs, while we allowed for statistically negative ones. At >30 mÅ, there is however a small offset in our respective scales caused by our non-treatment of the iron blend, such that (B24-B18)=7.50±8.55 mÅ. We therefore directly subtracted this constant mean value (7.50 mÅ) when calculating lithium-based ages. This offset is at worst five times smaller than the astrophysical scatter present in lithium EWs for calibration clusters at any given age (see Jeffries et al. 2023).

3. STELLAR PROPERTIES

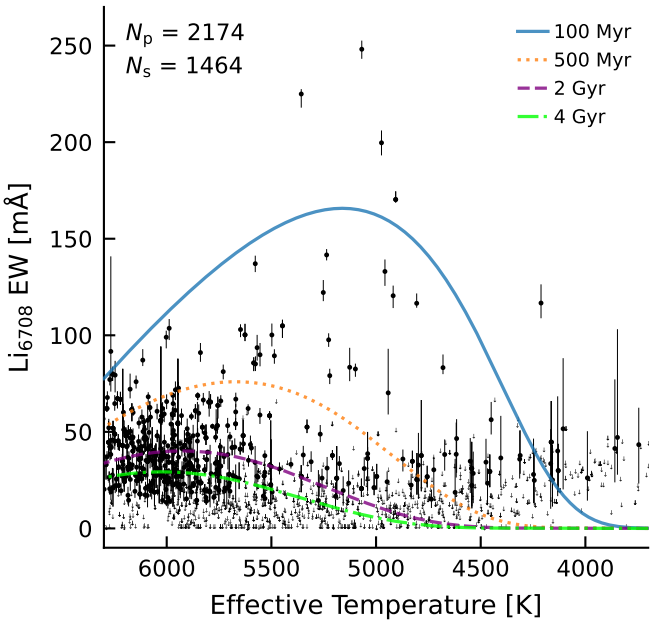

Figure 3. Equivalent widths (EW) of the Li I 6708 Å doublet for planet-hosting stars. These measurements were made from Keck/HIRES spectra collected from 2009–2024. Lines are the "mean" isochrones from Jeffries et al. (2023). The intrinsic dispersion around these isochrones becomes much larger than changes in the mean at $\gtrsim$1 Gyr (see Figure 4). Some stars with lithium detections do not have detected rotation periods, and vice-versa.

Our default source for stellar temperatures and surface gravities was the Gaia-Kepler Stellar Properties Catalog (GKSP; Berger et al. 2020b). The GKSP parameters were reported for stars with "AAA" 2MASS photometry, measured parallaxes in Gaia DR2, and *g*-band photometry available from either SDSS or else Kepler-INT (Greiss et al. 2012). The parameters themselves were derived using `isoclassify` (Huber et al. 2017) to interpolate over the MIST isochrone grids (Choi et al. 2016; Dotter 2016), given the SDSS *g* and 2MASS K_s photometry, the Gaia DR2 parallaxes, and *V*-band extinction from the Green et al. (2019) reddening map. The resulting stellar parameters are available for ≈94% of the 53,663 Kepler stars with rotation periods. For the remaining ≈6% of stars that lack temperatures and surface gravities from B20, we adopted the values reported by Santos et al. (2019) and Santos et al. (2021), which are primarily derived from the photometric Mathur et al. (2017) DR25 Kepler Stellar Properties Catalog. In the planet sample, ≈92% of the non-false-positive KOIs with rotation periods have parameters from Berger et al. (2020b), and the remainder are drawn from DR25.

David et al. (2021) compared the photometric B20 stellar parameters ($T_{\rm eff}$, $R_\star$, [Fe/H]) against the spectroscopic parameters from Fulton & Petigura (2018). The temperature scales showed a few-percent systematic difference, with F18 quoting higher temperatures than B20 for mid K dwarfs, and

lower temperatures for early F dwarfs. Our age analysis, described below, adopts the maximum of the two-sided uncertainties reported by B20 as a symmetric Gaussian temperature uncertainty. Systematic uncertainties in the temperature scale generally influence our age uncertainties at a smaller level than the statistical intrinsic scatter in the open cluster rotation sequences.

4. AGES FROM ROTATION

We calculated gyrochrone ages using `gyro-interp` (`v0.6`; Bouma et al. 2023), which is a method designed to address the fact that stars with the same mass and same rotation period can have a wide range of ages (e.g. Gallet & Bouvier 2015). The gyrochrone age posterior should therefore incorporate the intrinsic population-level scatter into its statistical precision. Figure 4 highlights this problem, particularly in regions where the 0.1–1 Gyr stars overlap.

To estimate the stellar spin-down rate as a function of time and stellar temperature, `gyro-interp` uses measured rotation periods and effective temperatures from reference open clusters, and interpolates between them using cubic Hermite polynomials. We calculated the probability of the rotation-based age, $t_{\rm gyro}$, given the observed periods and temperatures (and their uncertainties) by integrating Equation 1 of Bouma et al. (2023). This procedure marginalizes over the astrophysical scatter that is observed in the open cluster sequences. We adopted a linear age grid spanning 0–5 Gyr with 500 grid points, and interpolated the resulting posteriors to calculate any summary statistics. The oldest cluster for which `gyro-interp` is calibrated in `v0.6` is the 4 Gyr M67 cluster (Dungee et al. 2022; Gruner et al. 2023). For stars with rotation periods above the M67 sequence, our resulting age constraints are therefore quoted as lower limits.

Finally, we opted to modify `gyro-interp` in `v0.6` to incorporate an age-dependent population-level Gaussian scatter, as detailed in the change log at gyro-interp.readthedocs.io. While age precisions at $\leq$1 Gyr are unaffected, this update accounts for the observed intrinsic scatter in Ruprecht-147 and M67 being larger than in Praesepe or NGC-6811, potentially due to differential rotation (e.g., Epstein & Pinsonneault 2014). For $\approx$2-4 Gyr old stars with rotation periods measured at $\approx$5% precision, this change yields a $\lesssim$50% increase in age uncertainties.

4.1. *Stellar Quality Flags*

We calculated gyrochrone ages for all 45,229 stars with reported rotation periods that had effective temperatures of 3800–6200 K. To identify stars for which we suspect these ages may not be valid, we then built a set of quality flags which we condensed into a single binary number: $Q_{\rm star}$. When and how this bitmask should be applied depends on the question being asked. If the goal is to construct a false-positive free sample, all the quality flags could be applied. If the goal is to construct a complete sample, then consider the examples of Kepler 1627Ab ($\approx$40 Myr) and Kepler 51c ($\approx$625 Myr). The former has a high RUWE due to a resolved binary companion (Bouma et al. 2022a); the latter is on a grazing orbit (Masuda 2014). We leave selection for or against such cases as a decision to the user. For our own analysis, we assume that a star is suitable for gyrochronology if none of bits zero through ten (inclusive) are raised. For analyses that require all stellar rotation periods to come from the same detection pipeline, we further require bit 12 to be zero.

Three assumptions must hold for a rotation-based age dating method like `gyro-interp` to be valid. *1)* The evolutionary state of the star must be well-specified by its temperature and its age, *2)* the star's spin-down must not be influenced by binary companions, and *3)* the rotation period distribution for field stars of a given temperature and age must be identical to that of equally aged open clusters (metallicity differences, for instance, are ignored). A rephrasing of the first condition is that the star must be "near the main sequence" because during the post main sequence stellar temperatures change. From $\approx$0.08 to $\approx$3 Gyr, the stars of interest in this work (3800–6200 K, 0.5–1.2 $M_\odot$) have temperatures constant to $\approx$1% (Choi et al. 2016). From $\approx$3–4 Gyr, a 1.2 $M_\odot$ star's temperature drops from $\approx$6200 K to $\approx$6000 K ($\approx$3%), because its outer layers expand as it begins hydrogen shell burning as a subgiant. We treat this issue in a manner discussed in "bit 9" below.

Temperature range (bit 0)—We require stars to have effective temperatures $T_{\rm eff}$ between 3800 and 6200 K in order to report gyrochrone ages (Bouma et al. 2023). Stars hotter than 6200 K spin down very slowly, if at all. Stars cooler than 3800 K do spin down over gigayear timescales (Newton et al. 2016; Engle & Guinan 2023; Chiti et al. 2024), but the currently available open cluster data have yet to clarify when the intrinsic scatter in the population decreases.

Surface gravity (bit 1)—We flagged stars as possible subgiants if they had $\log g < 4.2$.

Absolute luminosity (bit 2)—We calculated the absolute Gaia DR3 G-band luminosity, ignoring reddening, using the reported apparent G-band magnitude and parallaxes. We flagged stars with $M_{\rm G} < 3.9$ or $M_{\rm G} > 8.5$, corresponding to main-sequence spectral types earlier than $\approx$F8V or later than $\approx$M0.5V (Pecaut & Mamajek 2013).

Known eclipsing binaries (bit 3)—We flagged any stars reported to be in the final Kepler eclipsing binary catalog (KEBC; Kirk et al. 2016).

Kepler-Gaia crossmatch quality (bits 4 and 5)— To leverage Gaia DR3 data, we used M. Bedell's 4″ Kepler-to-Gaia crossmatch of the NEA `q1_q17_dr25_stellar` catalog with Gaia DR3 (available at https://gaia-kepler.fun). The separation distribution of the Kepler-Gaia DR3 crossmatches is such that 99.2% of candidate matches are within 1″. We nonetheless noted an upturn in the candidate match rate from 3-4″; such sources are flagged using bit 4. For KIC stars with multiple potential Gaia matches within the 4″ radius, we adopted the brightest star as the default match. In most such cases this was unambiguous because there is a large brightness difference between the primary and any apparent neighbors. However cases with multiple stars within 4″ within ΔG<0.5 mag are noted using bit flag 5.

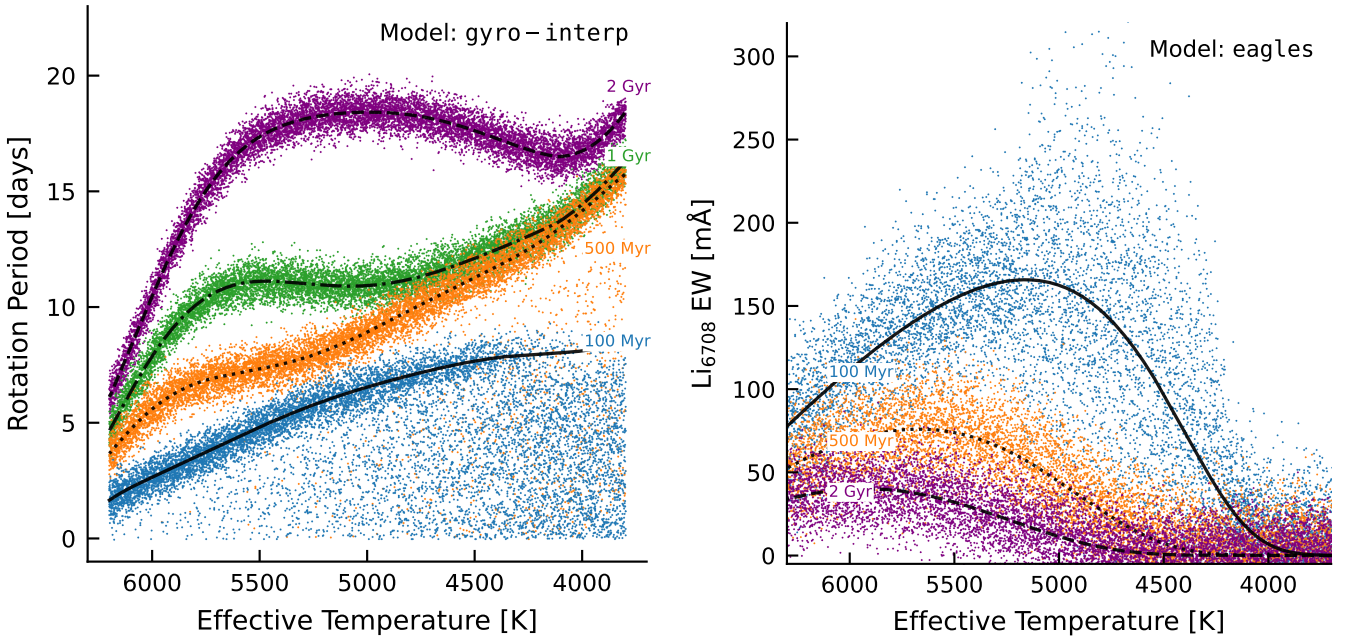

Figure 4. The models. Points represent 10^4 draws from models that have been fitted to rotation periods (Bouma et al. 2023) and lithium equivalent widths (EWs; Jeffries et al. 2023) of stars in open clusters. Lines are the "mean models" at various ages. The intrinsic dispersion around the mean, which is what the models fit, sets the theoretical precision floor for the age-dating methods. Additional sources of uncertainty, including measurement uncertainty, impose further limits on achievable precision. These models are calibrated using data from open clusters. The sizes of the points are the same in each panel, so that low apparent density signifies greater dispersion around the mean.

Gaia DR3 non-single-stars (bit 6)—The Gaia DR3 `non_single_star` column in the `gaia_source` table flags known eclipsing, astrometric, and spectroscopic binaries. We directly included this column.

RUWE (bit 7)—We inspected diagrams of the Gaia DR3 renormalized unit weight error (RUWE) as a function of other stellar parameters, and flagged stars with RUWE>1.4 as possible binaries. Such astrometric outliers can be either bona fide astrometric binaries, or more often are marginally resolved point sources for which a single-source PSF model provides a poor fit.

Crowding (bit 8)—We searched the Gaia DR3 point source catalog for stars within 1 Kepler pixel (4″) of every target star. While such companions may not not be physically associated with the target star, their presence can confuse rotation period measurements. We therefore flagged any stars with neighbors down to $1/10^{\text{th}}$ the brightness of the target star within this region (ΔG<2.5). We also considered a deeper cut (ΔG<5), and found it had negligible impact on our conclusions.

Near the main sequence (bit 9)—Figure 1 shows that many stars observed by Kepler are far from the main sequence. Some of the challenges this introduces for rotation-based ages include unresolved binaries, metallicity, reddening, and drivers of rotation other than magnetic braking. After exploring various options, we settled on the orange locus in the $\log g$–T_{eff} plane shown in Figure 1 as a way of flagging unresolved binaries, as well as evolved late-F and early-G stars. While the exact details of how this locus is constructed are arbitrary (see Appendix B), the general aim is to flag stars for which there is evidence based on their location in the HR or Kiel diagrams that our gyrochronology model may not be reliable. While the $\log g$–T_{eff} cut flags about half of Kepler stars with rotation periods as potentially not being suitable for gyrochronology, a few outliers in M_{G} vs. G_{BP}-G_{RP} remained after applying it. Such outliers are likely also questionable. We therefore also fitted a polynomial to the KOI main sequence in M_{G} vs. G_{BP}-G_{RP}, and flagged stars more than 1 magnitude from this locus as part of the same bitflag.

Metallicity (bit 10)—Theoretical models suggest that stars with non-solar metallicities spin down at different rates than solar-metallicity stars (Amard & Matt 2020). This expectation has been hard to verify due to a dearth of nearby non-solar metallicity open clusters. However, if true, this effect could cause systematic biases for gyrochrone ages (e.g. Figure 9 of Claytor et al. 2020). We therefore flagged stars with spectroscopic $|[\text{Fe}/\text{H}]|$>0.3 from either LAMOST DR5 (Zong et al. 2018) or CKS (Petigura et al. 2022) as being outside the range of our gyrochronology calibration. We discuss limitations of this approach in Section 8.

Candidate pulsators and close-in binaries (bit 11)—Santos et al. included in a flag for candidate "classical pulsators" (e.g. Cepheids) and close-in binaries. Visual inspection shows that although this flag selects many bona fide objects in these classes, it also selects most known young planets with $P_{\text{rot}} \lesssim 5$ day. These objects are neither classical pulsators nor close binaries. While we propagated this flag into our set of quality flags, we therefore generally ignore it.

Not in the homogeneous stellar rotation sample (bit 12)—This flag was set for the KOIs with rotation periods drawn from a source other than the Santos et al. pipeline.

4.2. *Planet Quality Flags*

Some planets are more reliably identified than others. We used the following additional quality indicators to assess the reliability and utility of a planet, and assembled them into a separate bitmask, $Q_{\rm planet}$.

Candidate reliability (bit 0)—The NEA's Kepler Objects of Interest Table includes both an overall planet-candidate disposition status (*koi_disposition*), as well as a disposition based only on the Kepler data (*koi_pdisposition*). We required both to include only "planet candidates" and "confirmed planets."

Candidate S/N (bit 1)—In any transit survey, the false positive rate increases greatly toward the noise floor for planet detection (e.g. Jenkins et al. 2002). We required a S/N in excess of Kepler's usual 7.1σ floor, through a cut on the maximum "multiple event statistic" (MES, *koi_max_mult_ev*): we required MES$>$10.

Grazing planets (bit 2)—Grazing objects, for which the impact parameter b is greater than $1-R_{\rm p}/R_\star$, often yield biased planetary parameters (e.g. Gilbert 2022). For large planets, they also include astrophysical false positives at higher rates (Morton et al. 2016), in part due to the size-impact parameter degeneracy. We flagged planet candidates as potentially grazing if $b>0.8$, using the impact parameters reported by Thompson et al. (2018).

5. AGES FROM LITHIUM

Figure 3 shows our measured equivalent widths for the lithium 6708 Å absorption doublet, plotted over the mean isochrone models from `EAGLES` (Jeffries et al. 2023). We show an upper-limit for plotting purposes if the 1σ lower limit on the equivalent width is below 10 mÅ. Our measured EWs span -40 to 250 mÅ; all negative EWs have uncertainties that are statistically consistent with zero.

To calculate lithium ages, we used `EAGLES` (git commit `ac09637`), which, similar to `gyro-interp`, is based on an empirical interpolation approach. `EAGLES` was calibrated on lithium measurements of stars observed by the Gaia-ESO spectroscopic survey in 52 open clusters with ages spanning 2 to 6,000 Myr (Jeffries et al. 2023). We adopted a linear prior in age, spanning 10^6 to 10^{10} yr, and symmetrize our EW uncertainties for purposes of interfacing with `EAGLES` by taking the maximum of the measured positive and negative 1σ uncertainty intervals.

In part because many of our EWs are upper limits, many of the lithium ages are lower limits. In such cases, the inferred age posterior is strongly influenced by the assumed intrinsic dispersion in the lithium model, and by the prior. In these instances, we quote the 3σ ($99.7^{\rm th}$ percentile) limits.

6. CLUSTER AGE COMPARISON

Stars that formed in the same birth cluster are the gold standard for the astronomical age scale (Soderblom 2010). Before Gaia, the few open clusters known in the Kepler field had been cataloged by Herschel (1864). Gaia has enabled the discovery of new stellar ensembles that are more diffuse, but which nonetheless share a common age based on isochrone, rotation, and lithium dating. Specifically in the Kepler field, NGC6811 (1 Gyr; Curtis et al. 2019) and NGC6819 (2.5 Gyr; Meibom et al. 2015) have been known for centuries, while Theia 520 ($\approx$300 Myr; Kounkel & Covey 2019), Melange-3 ($\approx$150 Myr; Barber et al. 2022), and Cep-Her ($\approx$40 Myr; Bouma et al. 2022b and Kerr et al. 2024 submitted) are more recent discoveries.

In Figure 5, we compare our rotation-based ages, and available ages from the literature, against the ages of stars in these open clusters. From the literature, we drew ages from Reinhold & Gizon (2015), Berger et al. (2020b), Lu et al. (2021), Mathur et al. (2023), and Lu et al. (2024). We followed any guidance available from each study for removing ages that were unreliable, and plotted stars within 1σ of zero as upper limits. For the Reinhold & Gizon ages, we used those calculated using the Mamajek & Hillenbrand (2008) calibration; for the Mathur et al. ages, we show those from `kiauhoku` (Claytor et al. 2020) rather than `STAREVOL` (Amard et al. 2019), since the former showed better agreement with the cluster age scale.

Cluster membership is a nuanced subject. Figure 5 is showing reported ages for a set of spatially and kinematically selected stars that could be cluster members, or they could be field interlopers. For NGC6811 and NGC6819, we adopted candidate members from Cantat-Gaudin et al. (2018, 2020) and Kounkel et al. (2020). For Theia 520, we used candidate members from Kounkel et al. (2020). For Melange-3, we used the candidates reported by Barber et al. (2022) and required "offset" tangential velocities below 2 km s^{-1}. For Cep-Her, we used candidate members from Kerr et al. 2024 (submitted) with $P_{\rm fin}>0.8$. Even with contaminants, we can compare the relative age distributions derived by the different studies because in all instances we are comparing reported ages against a fixed list of stars.

There are two main metrics for success in this test. *1)* Do the reported ages agree with the cluster age? *2)* Do the reported age uncertainties agree with their dispersion around the cluster age?

Figure 5 show that although previous studies reported ages that agree with the cluster scale for $\gtrsim$1 Gyr stars, subgigayear stars have historically had their ages overestimated by 0.3–2 dex, with severely understated uncertainties. For isochrone and kinematic ages, this is because these methods rely on parameters that do not appreciably change at $t\lesssim$1 Gyr. For the rotation-based ages in Mathur et al. (2023) and Lu et al. (2024), the discrepancy is caused by details of the calibration methodologies. The `kiauhoku` spin-down model for instance has known "stretches" and "compressions" in its age scale relative to observed open clusters (see Mathur et al. 2023, Sec. 7.3). The Mamajek & Hillenbrand (2008) calibration used by Reinhold & Gizon (2015) appears more accurate than the former two models, because it was fitted to reproduce the open cluster sequences known at the time.

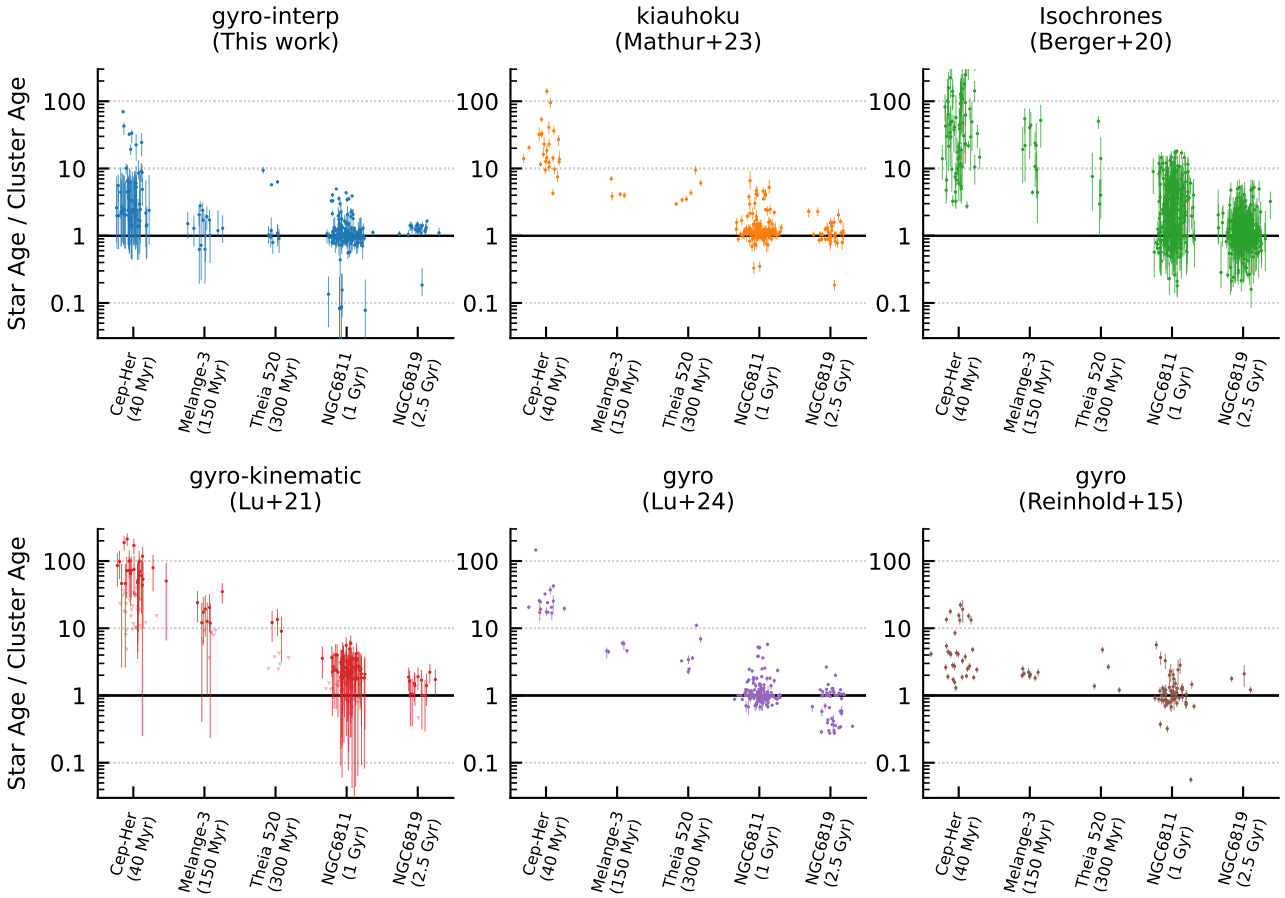

Figure 5. Reported ages of individual stars in benchmark open clusters. Each point denotes a star's reported age, normalized by the age of a stellar ensemble in which the star is a candidate member. Cluster membership was evaluated without knowledge of rotation. Although some field interlopers may be present in the membership lists, outliers can be compared between different methods on a relative basis. Each study was cross-matched against the same cluster list; certain methods report ages for more stars than others. Horizontal scatter is added to visually clarify the statistical age uncertainties. At <1 Gyr, our ages are generally accurate, and their statistical uncertainties match their dispersion.

However, the uncertainties from all of these methods appear to be underestimated. This is probably because they do not marginalize over the range of rotation periods accessible to sub-gigayear stars of a fixed mass and age.

7. RESULTS

7.1. *A Paucity Of Young Stars And Planets*

The stellar ages are given in Table 1 for the known planet hosts, and in Table 2 for all Kepler stars. Figure 6 shows the rotation-based age distributions of all the stars (left column) and the KOI hosts (middle column). These "histograms" are sampled from the posterior probability distributions by drawing ten random samples from each posterior, and then computing the normalized histogram of the resulting samples. We also considered an alternative approach for constructing these plots using hierarchical Bayesian deconvolution (Masuda et al. 2022), and found similar results. The plotted uncertainties assume Poisson statistics. We truncated the plots at 4 Gyr, which is the upper bound for our rotational age calibration. The overall slope yields a paucity of young stars relative to the expectation of a uniform age distribution.

The age distributions of Kepler stars and KOI hosts in Figure 6 appear similar. One diagnostic for whether the two distributions are drawn from the same underlying distribution is the Kolmogorov-Smirnov test; we calculated this statistic in a manner that accounts for the Poisson uncertainties by performing 1000 random draws of 70% of the stars from each sample when requiring $t_{\rm gyro}<3$ Gyr. The resulting $\log_{10} p$ values spanned ($2.5^{\rm th}$ to $97.5^{\rm th}$ percentiles) -4.5 to -1.8 for the K dwarfs, and -4.5 to -1.9 for all Kepler stars. This agrees with the visual impression that while small differences may be present, they are not drastic.

The similarity of the KOI host and Kepler star age distributions adds some nuance to the argument that young transiting planets are hard to detect due to the photometric variability of their host stars. If true, this statement seems to hold only for the very youngest ($\lesssim$0.4 Gyr) stars, where there is a marginal deficit in the KOI host age distribution relative to the parent stellar sample. Examining scatter plots of the planet properties as a function of age, we similarly find that fewer systems at $t_{\rm gyro}<0.4$ Gyr are detected with $P_{\rm orb}\gtrsim30$ days than at $t_{\rm gyro}>0.4$ Gyr.

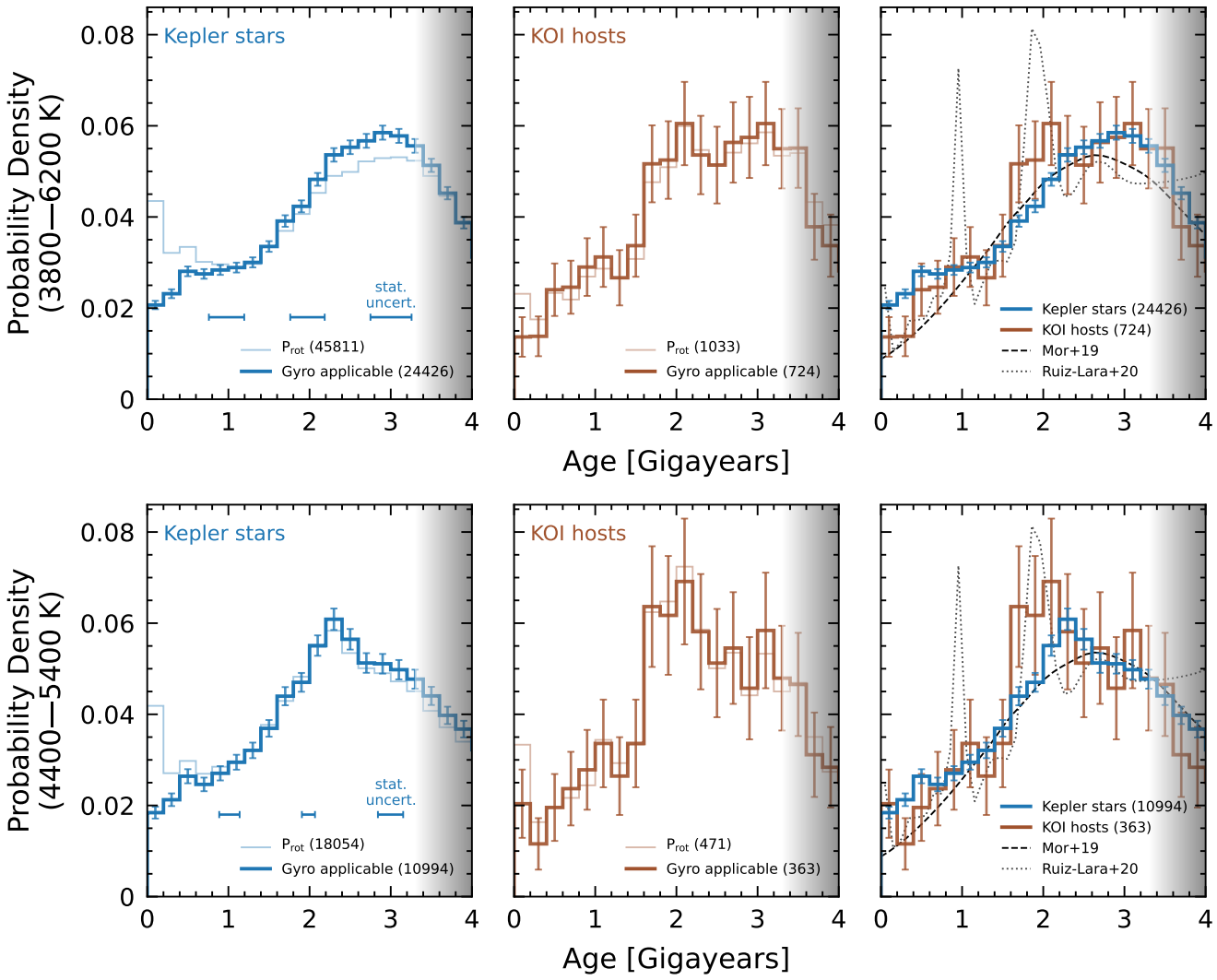

Figure 6. Kepler's demographic cliff, visible in the rotation-derived age distributions of its stars (left) and planet hosts (middle). The top row shows all stars with temperatures of 3800–6200 K for which we calculated rotational ages. Opaque lines impose quality cuts on binarity, metallicity, crowding, and the star's evolutionary state; transparent lines do not. The bottom row shows stars with temperatures of 4400–5400 K, which often have more precise ages. The statistical uncertainty for a mean star at 1, 2, and 3 Gyr is shown, and is identical across each row. Finally, the right panel compares the rotation-derived ages against star formation histories derived using CMD fitting (dashed and dotted lines). Completeness in Kepler's $P_{\rm rot}$ detection sensitivity is near unity until $t \lesssim 3$ Gyr (Masuda 2022a).

An important separate selection effect concerns Kepler's ability to detect the rotation signals. Masuda (2022a) studied this issue, and found for Sun-like stars that the fraction of rotation signals detectable by Kepler is near unity up to ≈3 Gyr, and that it drops to almost zero by ≈5 Gyr. This trend is opposite in functional form to our derived age distributionsand most of the stars in our sample are indeed G dwarfs (see e.g., the $t_{\rm gyro}$–$T_{\rm eff}$ distributions in Appendix D).

We can quantify the relative counts of stars as a function of age by labelling stars between 0-1 Gyr, 1-2 Gyr, and 2-3 Gyr as "young", "intermediate-age", and "old". A simple counting exercise from Figure 6 tells us that there are 2.1 times as many old stars in the Kepler field as young stars. Similarly, there are 2.6 times as many old planet hosts as young planet hosts. Focusing only on the tails of the distributions (0-0.3 Gyr and 2.7-3 Gyr), the implication is that the formation rate of stars in the Kepler field decreased by a factor of 2.81±0.12 over the past three billion years. If this decrease continues linearly into the future, then a simple extrapolation would imply that in ≈1.4±0.3 Gyr the rate of new stars forming in the Galaxy will reach zero.

In terms of detected planet counts, our rotation-based ages for the Kepler sample yield {109, 201, 281} detected planets in the 0-1 Gyr, 1-2 Gyr, and 2-3 Gyr bins.

7.2. *Planets Younger Than One Billion Years*

Sub-gigayear planets can be particularly informative for studies of planet evolution. Our catalog has 109 confirmed

and candidate planets with median ages below 1 Gyr. Requiring $t_{\rm gyro}$<1 Gyr at 2σ yields 63 planets orbiting 50 stars. The youth claim is most secure for the systems that are either in clusters (Section 7.2.1), or that have independent rotation and lithium-based ages (Section 7.2.2). These samples provide broader context for the planets around field stars that push the boundaries of the current young exoplanet census (Section 7.2.3).

7.2.1. *Planets in Clusters*

Four stellar ensembles in the Kepler field have to date yielded a total of fourteen transiting planets. Our analysis blindly recovers the youth of all of these planets.

Cep-Her—The Cep-Her complex (≈40 Myr) contains Kepler-1627Ab, Kepler-1643b, Kepler-1974b and Kepler-1975 Ab (Bouma et al. 2022a,b). Different sub-groups of the complex vary in age by ≈50% (Kerr et al., submitted). The planets themselves are all on close-in orbits (5-25 days), with sizes from 2-4 $R_\oplus$. Our rotation and lithium ages agree with the cluster age for Kepler-1627A, Kepler-1974, and Kepler-1975A. For Kepler-1643, the rotation and cluster ages agree, and the lithium age is 2.0σ above the cluster age reported by Bouma et al. (2022b) for RSG-5.

MELANGE-3—Barber et al. (2022) reported a 105 ± 10 Myr association in the Kepler field containing two transiting mini-Neptunes: Kepler-970 and Kepler-1928. We find rotation-based ages of $t_{\rm gyro}$ = 176^{+120}_{-40} Myr and 144^{+104}_{-88} Myr for Kepler-970 and Kepler-1928 respectively. The former rotation-based age being slightly older than the suggested Pleiades age for the association agrees with Figure 4 of Barber et al. (2022).

Theia 520—We find rotation-based ages of ≈350 Myr for Kepler-968 and Kepler-52. Based on spatial and kinematic clustering, these stars are candidate members of Theia 520 (Kounkel & Covey 2019). The core of this cluster is also known as UBC-1 (Castro-Ginard et al. 2018). Based on isochrone and rotation-based age-dating, Theia 520 seems to be ≈230±70 Myr old (Fritzewski et al. 2024), which is within 1σ of our $t_{\rm gyro}$ measurements. Ongoing work by Curtis (2024) broadly finds that the two planet-hosting stars are indeed members of this diffuse population. Given the cluster-level and individual-star evidence, this makes Kepler-968 and Kepler-52 the youngest multiplanet systems currently known from the main Kepler mission.

NGC 6811—Meibom et al. (2013) reported the discovery of Kepler-66 and -67b, two mini-Neptunes in NGC 6811 (≈1 Gyr). We derive rotation-based ages for these systems of 1431^{+675}_{-364} Myr and 878^{+108}_{-121} Myr for Kepler-66 and -67b, respectively. Kepler-66 ($T_{\rm eff}$≈5900 K, $P_{\rm rot}$≈10.4 days) has a lower precision and a more asymmetric posterior because of its slow spin-down rate. Kepler-67 ($T_{\rm eff}$≈5100 K, $P_{\rm rot}$≈10.3 days) is marginally hotter than the later K dwarfs that are in "stalled" spin-down at this time, enabling its rotation period to be diagnostic of its age.

7.2.2. *Rotation vs. Lithium Ages*

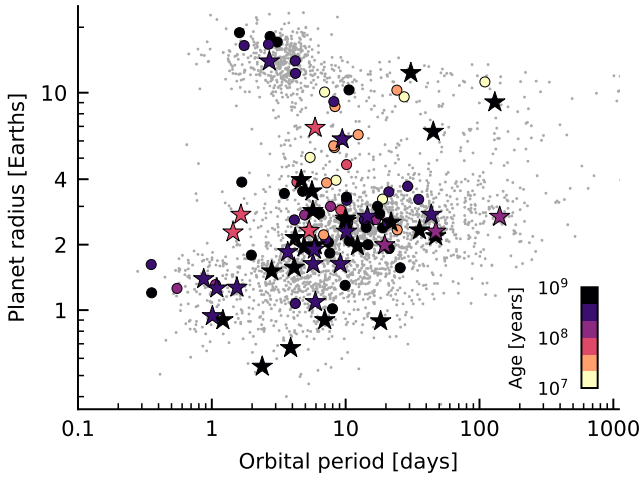

Figure 7. Sizes, orbital periods, and rotation-based ages of transiting exoplanets younger than one billion years. Star symbols denote 46 planets that are characterized in this work to have $t_{\rm gyro}$<1 Gyr at 2σ; circles are planets from the literature meeting the same age requirement, but with a heterogeneous set of age provenances. Gray points are transiting planets from the NASA Exoplanet Archive older than 1 Gyr. If one were to instead select for precise ages ($t/\sigma_t > 3$), this would hide ≈ten <0.5 Gyr planets, and add ≈fifteen 0.5-1 Gyr planets. For this plot, we require our Kepler stellar hosts to not have $Q_{\rm star}$ bits 0–9 raised, and for the planets to similarly no have quality flags raised.

We compared the rotation and lithium ages for the known planet hosts in the "Consistent?" column of Table 1. There were three cases of interest. *i)* If two-sided posteriors for both $t_{\rm gyro}$ and $t_{\rm Li}$ existed, and their median values were consistent within 2σ, we listed them as consistent; if they were consistent within 2-3σ, we listed them as "maybe" consistent. Otherwise, they disagreed. *ii)* If $t_{\rm Li}$ was a lower limit, we compared this lower limit with the 1σ upper limit from $t_{\rm gyro}$; if the two overlapped, we judged the age estimates to be consistent. *iii)* If $t_{\rm Li}$ provided a two-sided posterior, and no rotation period was found, we judged the age estimates to be inconsistent. This is because a two-sided lithium constraint can only be provided for G and K dwarfs $\lesssim$2 Gyr old, and Kepler should have been sensitive to the rotation periods of such stars.

In the entire planet sample (i.e. without imposing any quality cuts) this yielded 697 consistent cases, 12 maybe consistent cases, and 22 inconsistent cases. Rephrased, in the overall sample, 95% of stars have consistent rotation and lithium-based ages (97% potentially consistent).

Appendix C describes all cases of "discrepant" confirmed planets for which a sub-gigayear age is reported by at least one age indicator. All but two systems are either evolved stars or else unresolved binaries, and are automatically flagged as such. The more interesting of the two is Kepler-786, an early K dwarf with $t_{\rm Li}$=228^{+168}_{-87} Myr, but with a ≈33 day rotation period that implies $t_{\rm gyro}$≈4.4,Gyr. Other age indicators in the

spectrum similarly suggest that the star is not young. It therefore appears to be anomalously lithium-rich.

7.2.3. *Notable New Young Planets*

Let us focus on blemish-free stars with blemish-free planets: $Q_{\rm star}$ must not have any of bits zero through ten raised, and $Q_{\rm planet}$ must similarly have no quality flags raised. Under this constraint, our results include 18 confirmed planets younger than 1 Gyr with two-sided $t_{\rm gyro}$ and $t_{\rm Li}$, and 37 confirmed planets with comparable ages for which $t_{\rm gyro}$ is two-sided while $t_{\rm Li}$ is one-sided.

Figure 7 shows the planets and planet candidates with $t_{\rm gyro}<1$ Gyr at 2σ. This figure includes 37 confirmed Kepler planets, and nine candidate planets, all of which are listed in Table 1. These include seven objects Earth-sized or smaller, two Jovian-sized planet candidates, four super-Neptunes (4–10 $R_\oplus$), 22 mini-Neptunes above the radius valley as parametrized by Van Eylen et al. 2018, and 14 super-Earth sized planets below the radius valley. While most of these planets are on orbital periods below 50 days, two are on more distant orbits.

Among these systems, four highlights are Kepler-1529, Kepler-1565, Kepler-1312, and Kepler-1629. Kepler-1529b is a $\approx$100$\pm$50 Myr mini-Neptune with well-measured rotation and lithium ages. Kepler-1565b is an analogous $\approx$170-230 Myr super-Earth. Kepler-1312 is a $t_{\rm gyro}=357^{+75}_{-109}$ Myr near-Solar analog with an Earth-sized planet on a one-day orbit, and a mini-Neptune on a five-day orbit. The Earth-sized planet, Kepler-1312 c, along with the near-identical Kepler-1561 b ($t_{\rm gyro}=426^{+74}_{-78}$ Myr), rank among the youngest Earth-sized planets currently known, comparable to planets such as HD 63433d (1.1 $R_\oplus$, 414$\pm$23 Myr; Capistrant et al. 2024) and TOI-1807 b (1.3 $R_\oplus$, 180$\pm$40 Myr; Hedges et al. 2021). Kepler-1629 b, with a size just two-thirds that of Earth (0.67$\pm$0.05 $R_\oplus$), is marginally older, also based on rotation (529^{+62}_{-62} Myr). The lithium age from a reconnaissance TRES spectrum confirms the point.

8. DISCUSSION

8.1. *The Thin Disk's Star Formation History*

Most of the stars observed by Kepler are in the thin disk. This can be verified by following Gaia Collaboration et al. (2018), and labeling stars with 2D tangential velocities $v_{\rm T}<40$ km s^{-1} as thin disk members, and those with $60<v_{\rm T}<150$ km s^{-1} as thick disk members. For all stars in the KIC, this yields 95,694 thin and 54,039 thick disk stars respectively. The thin disk stars have a threefold larger detected rotation period fraction: 35,675 rotators are in the thin disk, while 7,312 are in the thick disk. Further imposing the gyrochronology quality flags discussed in Section 4.1 yields 17,755 thin-disk stars for which gyrochronology is applicable, and 2,462 thick-disk stars.

Classifying Kepler stars as thin vs. thick disk members helps connect them to previous work on the Galaxy's star formation history. On extragalactic scales, the star formation rate in spiral galaxies with mass similar to the Milky Way peaked $\approx$10 Gyr ago, and has since decreased by an order of magnitude (e.g. Heavens et al. 2004; Hopkins & Beacom 2006). In our own galaxy, previous studies have measured star formation histories through CMD fitting of resolved stellar populations (Mor et al. 2019; Ruiz-Lara et al. 2020; Alzate et al. 2021; Xiang & Rix 2022) and by modeling the local white dwarf luminosity function (e.g. Isern 2019). Mor et al. (2019) and Isern (2019) for instance focused on stars (and white dwarfs) within a few hundred parsecs, and both found a peak in the local star formation rate 2-3 Gyr ago. Ruiz-Lara et al. (2020) focused on stars in a wider 2 kpc bubble, and additionally reported three local maxima in the galactic star formation rate, which they associated with pericenter passages of the Sagittarius satellite galaxy.

The right column of Figure 6 compares our derived age distribution against star formation histories (SFHs) reported by Mor et al. (2019) and Ruiz-Lara et al. (2020) based on CMD fitting. The overall slope of both SFHs broadly agrees with what we find from rotation-based ages. The SFH from Mor et al. (2019) seems entirely consistent, particularly after accounting for the statistical uncertainties of that study. Regarding the episodic star formation bursts reported by Ruiz-Lara et al. (2020), they are not apparent in our overall FGK star sample (top row). However, rotation-based ages are most precise for $\approx$G8V-K4V dwarfs older than $\approx$1.5 Gyr (Bouma et al. 2023). The lower row of Figure 6 selects these stars with a temperature cut, and may show a hint of the $\approx$2 Gyr spike reported by Ruiz-Lara et al. (2020). The $\approx$1 Gyr spike however is not recovered. This $\approx$2.5 Gyr local maximum is similarly present in the isochrone ages derived by Berger et al. (2020b) for the Kepler field, and in the red giant asteroseismic ages derived by Silva Aguirre et al. (2018). The main novelty of our ages relative to those studies is their improved accuracy at $<$1 Gyr.

8.2. *Caveats & Limitations*

Our most constraining ages tend to come from one source of information: rotation. Factors other than stellar age and mass can influence stellar rotation rates. Binarity is one example: even intermediate-separation ($\sim$10 AU) binaries are biased toward rapid rotation (e.g. Meibom et al. 2007, and many studies thereafter). Metallicity may also be relevant (Amard et al. 2020; See et al. 2024). An additional caveat is that our rotation-based ages used photometric effective temperatures (Section 3), even though spectroscopic temperatures are available for the planet-hosting subset. This decision was driven by a desire for homogeneity irrespective of planet-hosting status. However it implies that the estimated planet ages might shift if one were to account for the spectroscopic information.

We were interested in not only the overall age distribution of the Kepler field, but also in the reliability of individual ages for young stars known to host planets. We attempted to assess this reliability using quality bitmasks (Table 1), a comparison against cluster ages (Section 6), and a comparison between rotation and lithium ages. The cluster comparison suggested that our ages were generally accurate at

$\ll$0.5 dex across 0.04–2.5 Gyr, similar to their quoted precision. Nonetheless, the upper-left panel of Figure 5 does show outliers, typically $\lesssim$10% of the population in any cluster. These stars could be either field star contaminants, or else anomalous stars whose physical rotation histories were altered by processes not captured by our statistical uncertainties. Similarly, although we found $t_{\rm gyro}$ and $t_{\rm Li}$ to agree for 18 planets orbiting "high-quality" stars, we did find one system, Kepler-786, with radically different lithium (228^{+168}_{-87} Myr) and rotational ($\approx$4.4 Gyr) ages. Planetary mergers are one process that could produce such a signal, but testing this would require a method for measuring differential abundances across a large number of elements.

A separate plausible origin for rotational outliers is that they come from erroneously reported rotation periods. While the large surveys do show good internal consistency (Appendix E), the referee correctly pointed out that this is only a comparative test of methods, rather than an ability to recover ground truth (e.g. Aigrain et al. 2015). One could imagine an adversarial scenario in which, say, 10-20% of stars with $P_{\rm rot}>$20 days are erroneously reported, and in fact have much longer rotation periods. In this scenario, our analysis would overestimate the degree by which the SFR in the Kepler field has decreased, by 7-14%.

Other age indicators may help in verifying the ages of the $\lesssim$3 Gyr stars that are the main focus of this work. Specifically, chromospheric emission in the X-ray, Ca II HK line, and the UV can serve as an age tracer (Mamajek & Hillenbrand 2008; Vidotto et al. 2014; Engle 2024). However, these age indicators are all in a sense "rotation-powered". The dynamo converts kinetic energy into magnetic energy, which is emitted through these chromospheric pathways. We did not attempt to incorporate these indicators into this study due to concerns regarding sensitivity, homogeneity, and the question of whether they in fact provide age information that is truly independent from rotation.

A broader question, beyond the scope of this work, concerns the ages of stars $\gtrsim$4 Gyr old. For age-dating models based only on rotation rates, an important challenge is that the detectability of the rotation signals for 3-10 Gyr stars, especially Sun-like stars, is at the limits of the Kepler data (Masuda 2022a). In the "old star" regime, methods that leverage either asteroseismology (van Saders et al. 2016; Saunders et al. 2024), or else that combine both the evolution of stellar luminosity and stellar rotation (Angus et al. 2019; Claytor et al. 2020; Mathur et al. 2023) seem the most capable of providing useful age constraints for single stars over the full span of their main-sequence lifetimes.

8.3. *Future Directions*

Occurrence Rates: The age-dependent trends predicted for exoplanet populations, such as the Kelvin-Helmholtz cooling of mini-Neptunes (Gupta & Schlichting 2019), time-dependent carving of the photoevaporation desert (Owen & Lai 2018), and the time evolution of the radius valley (Rogers & Owen 2021) can be explored using our data. We defer this analysis to a separate publication. Some care is required since beyond age, exoplanet demographics also depend on stellar metallicity and mass (e.g. Petigura et al. 2018; Miyazaki & Masuda 2023).

Field star ages from other surveys: While this study focused on Kepler, other photometric surveys (e.g. K2, TESS, HAT, WASP, NGTS, ZTF, ATLAS) open opportunities for age-dating a far broader set of stars and planets. Future prospects also include PLATO (Rauer et al. 2014), Earth 2.0 (Ge et al. 2022), and the Roman Galactic Bulge Time Domain Survey (Wilson et al. 2023). Rotation-based age-dating from these surveys could yield new insight into whether the star formation history that we see in the Kepler field is universal across the thin disk.

Searches for new associations: Some of the youngest stars in Tables 1 and 2 have been linked to their birth clusters, while others have not. A systematic search for the birth clusters of the youngest "field stars" could combine positions and velocities from Gaia with rotation measurements from TESS. Given the $\sim$100 Myr decoherence time of young clusters, the youngest "field stars" may have easily identifiable young neighbors.

9. CONCLUSIONS

We began this work with two questions: how wrong is the assumption of a uniform age distribution for stars in the galactic thin disk? And why are only $\approx$50 sub-gigayear transiting planets known, rather than the $\approx$500 that would be expected under the assumption of a uniform star formation history for the $\approx$5,000 known planets?

Our approach to answering these questions was to curate a sample of stellar rotation periods, lithium equivalent widths, and temperatures using archival and new data from the Kepler field. We derived new ages using empirical interpolation-based methods, and assessed the reliability of these ages by comparing them against benchmark open clusters (Figure 5).

Tables 1 and 2 summarize the results for planets and stars, respectively. Our recovered ages are accurate for all 14 known Kepler planets in clusters. While lithium provided minimal added information for most of the sample, $t_{\rm Li}$ and $t_{\rm gyro}$ agreed in $\gtrsim$90% of cases for which comparison was possible. Our resulting ages included two-sided $t_{\rm gyro}$ and $t_{\rm Li}$ for 18 sub-gigayear confirmed planets, and two-sided $t_{\rm gyro}$ with one-sided $t_{\rm Li}$ for 37 sub-gigayear confirmed planets. Allowing for "candidate" planets, grazing transit geometries, and stars with RUWE far from unity expands the counts by a factor of two.

The sizes and periods for the most secure set of planets are shown in Figure 7. While the new young planets are mostly mini-Neptunes, some are near the lower boundary of the "sub-Jovian desert" (Owen & Lai 2018), which could have an evolutionary connection to their youth. Other discoveries include Earth-sized planets with new ages of only a few hundred million years.

Our main conclusions with respect to our original questions are as follows.

1. Rather than being uniform, the age distributions of both the Kepler target stars and the known Kepler planet-hosts show a demographic cliff. There are twice as many "old" (2-3 Gyr) stars in the Kepler field as "young" (0-1 Gyr) stars. The star formation rate today is 2.81 ± 0.12 times lower than it was three billion years ago. This result from rotation-based ages broadly agrees with recent reports of a declining star-formation rate from CMD fitting and white-dwarf chronology, though with the advantage of better sensitivity for FGK stars at $t<1$ Gyr (e.g. Figure 5).
2. Rather than expecting $\approx$500 exoplanets younger than one billion years, the age distribution of stars in the Kepler field suggests that we should instead expect $\approx$250.
3. We have derived rotation-based ages for 63 Kepler planets younger than 1 Gyr at 2σ, and 109 planets with median ages below 1 Gyr. Concatenating these planets against the existing literature yields $\approx$170 known sub-gigayear planets. This lessens the original factor of ten discrepancy to a factor of at most two.

ACKNOWLEDGMENTS

This work was supported by the Heising-Simons 51 Pegasi b Fellowship (LGB, EKP) and the Arthur R. Adams SURF Fellowship (EKP). The HIRES data were obtained at the Keck Observatory. We recognize the importance that the summit of Maunakea has always had within the indigenous Hawaiian community, and we are deeply grateful for the opportunity to conduct observations from this mountain.

Contributions: Per https://credit.niso.org/: Conceptualization: LGB. Data curation: LGB, AWH, HI. Formal analysis: LGB, KM. Funding acquisition: LGB. Investigation: LGB, EKP. Methodology: LGB, EKP, KM. Project administration: LGB, LAH, AWH. Resources: LGB, AWH. Software: LGB. Supervision: LGB, LAH. Validation: LGB, KM. Visualization: LGB. Writing – original draft: LGB. Writing – review & editing: all authors.

Facilities: Gaia (Gaia Collaboration et al. 2022), Kepler (Borucki et al. 2010), Keck:I (HIRES) (Vogt et al. 1994b), 2MASS (Skrutskie et al. 2006), SDSS (York et al. 2000).

Software: astropy (Price-Whelan et al. 2018), claude (Anthropic 2024), eagles (Jeffries et al. 2023), gyro-interp (Bouma et al. 2023), matplotlib (Hunter et al. 2007), numpy (Van Der Walt et al. 2011), scipy (Virtanen et al. 2020).

Table 1. Ages of Kepler planets and planet candidates. This version of the table is truncated to include the youngest systems, sorted by the minimum of either the rotation or lithium-based age. The full machine-readable table contains ages and age limits for 2,461 non-false positive KOIs with MES>10. A bash script to decode the Q_{star} quality flag is **available online**. A python script to select stars with specific bit flags is **also available**. All quoted age uncertainties are statistical.

KOI	Kepler	T_{eff}	P_{rot}	EW^*_{Li}	t_{gyro}	t_{Li}	Consistent?	R_p	P_{orb}	Q_{planet}	Q_{star}	Spec?	Comment
–	–	K	days	mÅ	Myr	Myr	str	Earths	days	int	int	bool	–
K05245.01	Kepler-1627 b	5357	2.62	225 ± 7	81^{+158}_{-55}	51^{+38}_{-27}	Yes	3.79	7.2	0	2176	1	Cep-Her
K07368.01	Kepler-1974 b	5068	2.56	248 ± 4	88^{+183}_{-60}	54^{+47}_{-25}	Yes	2.22	6.84	0	2560	1	Cep-Her
K06228.01	Kepler-1644 b	5521	1.43	-2 ± 13	77^{+144}_{-53}	> 767	No	1.88	21.09	4	2690	1	Unres. Binary
K06186.01	Kepler-1643 b	4918	5.05	120 ± 6	79^{+182}_{-54}	191^{+92}_{-76}	Yes	2.11	5.34	0	0	1	Cep-Her
K03933.01	Kepler-1699 b	5496	4.16	-11 ± 7	85^{+106}_{-58}	> 889	No	1.32	3.49	0	2688	1	Unres. Binary
K03916.01	Kepler-1529 b	4974	6.43	200 ± 6	109^{+117}_{-71}	90^{+53}_{-39}	Yes	2.01	5.34	0	0	1	✓✓
K01804.01	Kepler-957 b	4947	4.52	24 ± 9	96^{+196}_{-66}	> 241	Yes	6.9	5.91	0	0	1	✓
K07913.01	Kepler-1975 b	4450	3.36	56 ± 9	96^{+223}_{-66}	> 57	Yes	2.03	24.28	0	2816	1	Cep-Her
K03936.02	Kepler-1930 b	4906	7.1	170 ± 4	174^{+106}_{-65}	115^{+55}_{-49}	Yes	1.52	13.03	4	0	1	
K03876.01	Kepler-1928 b	5577	4.64	137 ± 4	148^{+102}_{-87}	189^{+150}_{-94}	Yes	1.86	19.58	0	2048	1	MELANGE-3
K04069.01	Kepler-1938 b	4617	7.82	6 ± 16	152^{+112}_{-42}	> 208	Yes	1.47	13.06	0	2048	1	✓
K02678.01	Kepler-1313 b	5236	6.13	142 ± 3	197^{+112}_{-91}	174^{+96}_{-72}	Yes	1.71	3.83	4	2048	1	
K04194.01	Kepler-1565 b	4958	7.4	133 ± 7	230^{+111}_{-85}	174^{+81}_{-72}	Yes	1.27	1.54	0	0	1	✓✓
K03835.01	Kepler-1521 b	4806	7.82	117 ± 5	207^{+98}_{-68}	176^{+79}_{-69}	Yes	2.3	47.15	0	2048	1	✓✓
K01838.01	Kepler-970 b	4314	9.23	36 ± 14	177^{+124}_{-39}	> 92	Yes	2.15	16.74	4	0	1	MELANGE-3
K00063.01	Kepler-63 b	5486	5.49	89 ± 4	223^{+98}_{-92}	542^{+475}_{-256}	Yes	5.64	9.43	0	4096	1	✓✓
K01199.01	Kepler-786 b	4680	33.06	83 ± 6	4364^{+359}_{-374}	228^{+168}_{-87}	No	2.31	53.53	0	0	1	Mystery
K03316.01	Kepler-1467 b	5252	6.31	122 ± 6	230^{+112}_{-98}	236^{+151}_{-95}	Yes	3.11	47.06	0	0	1	✓✓
K01074.01	Kepler-762 b	5921	4.01	-27 ± 25	245^{+114}_{-100}	> 548	Maybe	15.19	3.77	0	512	1	
K01839.01	Kepler-971 b	5447	6.22	105 ± 6	306^{+95}_{-115}	366^{+290}_{-164}	Yes	3.93	9.59	0	128	1	
K01833.01	Kepler-968 b	4413	10.46	10 ± 18	328^{+108}_{-87}	> 159	Yes	1.85	3.69	0	0	1	Theia-520
K01833.03	Kepler-968 c	4413	10.46	10 ± 18	328^{+108}_{-87}	> 159	Yes	1.63	5.71	0	0	1	Theia-520
K01833.02	Kepler-968 d	4413	10.46	10 ± 18	328^{+108}_{-87}	> 159	Yes	2.28	7.68	4	0	1	Theia-520
K02675.01	Kepler-1312 b	5584	6.13	86 ± 4	357^{+75}_{-109}	642^{+617}_{-318}	Yes	2.07	5.45	0	4096	1	✓✓
K02675.02	Kepler-1312 c	5584	6.13	86 ± 4	357^{+75}_{-109}	642^{+617}_{-318}	Yes	0.94	1.12	0	4096	1	✓✓
K00775.02	Kepler-52 b	4164	11.85	22 ± 18	360^{+208}_{-97}	> 100	Yes	2.19	7.88	0	0	1	Theia-520
K00775.01	Kepler-52 c	4164	11.85	22 ± 18	360^{+208}_{-97}	> 100	Yes	2.04	16.38	0	0	1	Theia-520
K00775.03	Kepler-52 d	4164	11.85	22 ± 18	360^{+208}_{-97}	> 100	Yes	2.03	36.45	0	0	1	Theia-520
K04004.01	Kepler-1933 b	5576	6.21	85 ± 3	366^{+74}_{-109}	642^{+603}_{-318}	Yes	1.01	4.94	4	0	1	
K02174.03	Kepler-1802 b	4245	11.45	–	379^{+201}_{-109}	–	–	1.71	7.73	4	820	0	
K02174.02	Kepler-1802 c	4245	11.45	–	379^{+201}_{-109}	–	–	2.05	33.14	0	820	0	
K03935.01	Kepler-1532 b	5554	6.48	90 ± 6	397^{+71}_{-102}	567^{+545}_{-278}	Yes	1.26	1.09	0	0	1	✓✓
K01801.01	Kepler-955 b	5221	7.5	79 ± 4	397^{+99}_{-131}	536^{+481}_{-237}	Yes	2.69	14.53	0	0	1	✓✓
K01800.01	Kepler-447 b	5648	6.4	103 ± 3	420^{+64}_{-78}	405^{+355}_{-203}	Yes	18.49	7.79	4	2048	1	
K03370.02	Kepler-1481 b	4832	9.11	22 ± 7	407^{+126}_{-118}	> 210	Yes	1.09	5.94	0	0	1	✓
K04156.01	Kepler-1943 b	6002	–	99 ± 5	–	409^{+520}_{-254}	No	1.29	4.85	4	518	1	
K00448.01	Kepler-159 b	4511	10.5	19 ± 10	415^{+160}_{-110}	> 161	Yes	2.3	10.14	0	4096	1	✓
K00448.02	Kepler-159 c	4511	10.5	19 ± 10	415^{+160}_{-110}	> 161	Yes	2.75	43.59	0	4096	1	✓
K00046.01	Kepler-101 b	5498	–	100 ± 5	–	419^{+349}_{-196}	No	5.9	3.49	0	1542	1	
K04169.01	Kepler-1561 b	5742	6.18	66 ± 3	426^{+74}_{-78}	1409^{+1718}_{-788}	Maybe	0.94	1.01	0	2048	1	✓✓
K02708.01	Kepler-1320 b	4536	10.46	25 ± 32	430^{+173}_{-113}	> 140	Yes	1.39	0.87	0	0	1	✓
K00119.01	Kepler-108 b	5626	–	100 ± 5	–	438^{+402}_{-220}	No	8.2	49.18	0	418	1	
K00119.02	Kepler-108 c	5626	–	100 ± 5	–	438^{+402}_{-220}	No	7.78	190.32	4	418	1	
K00323.01	Kepler-523 b	5267	7.6	49 ± 4	444^{+87}_{-114}	1824^{+2706}_{-1047}	Maybe	1.9	5.84	0	0	1	✓✓
K02115.01	Kepler-67 b	5126	10.39	83 ± 10	878^{+108}_{-121}	458^{+451}_{-206}	Yes	2.96	15.73	0	0	1	✓✓
K00002.01	Kepler-2 b	6436	–	83 ± 4	–	485^{+924}_{-353}	–	16.42	2.2	0	7	1	
K03371.02	Kepler-1482 b	5330	7.7	52 ± 3	491^{+76}_{-91}	1630^{+2285}_{-904}	Maybe	1.0	12.25	0	640	1	

Table 1 *continued*

Table 1 *(continued)*

K03497.01	Kepler-1512 b	4894	9.33	14 ± 8	505^{+135}_{-115}	> 295	Yes	0.8	20.36	4	4738	1	
K03864.01	Kepler-1698 b	4866	9.49	2 ± 8	518^{+151}_{-123}	> 358	Yes	0.9	1.21	0	1024	1	
K03010.01	Kepler-1410 b	3808	14.19	-21 ± 24	523^{+612}_{-196}	> 80	Yes	1.39	60.87	0	512	1	
K05447.02	Kepler-1629 b	5585	7.45	–	529^{+62}_{-62}	–	–	0.67	3.88	0	0	0	
K04246.01	Kepler-1576 b	5794	7.09	17 ± 8	559^{+103}_{-71}	> 613	Yes	0.9	6.98	0	0	1	✓
K03324.01	Kepler-1469 b	5356	8.15	-5 ± 25	562^{+75}_{-82}	> 535	Yes	2.53	21.86	0	0	1	✓
K01779.01	Kepler-318 b	5799	7.09	65 ± 3	562^{+106}_{-72}	1507^{+1876}_{-858}	Yes	3.97	4.66	0	0	1	✓✓
K01779.02	Kepler-318 c	5799	7.09	65 ± 3	562^{+106}_{-72}	1507^{+1876}_{-858}	Yes	3.1	11.82	4	0	1	
K02084.01	Kepler-1792 b	4942	9.49	13 ± 11	587^{+155}_{-144}	> 312	Yes	2.15	4.2	0	0	1	✓
K02035.01	Kepler-1066 b	5847	7.0	60 ± 4	588^{+158}_{-85}	2018^{+2616}_{-1187}	Maybe	1.96	1.93	4	1024	1	
K03274.01	Kepler-1451 b	5675	7.82	42 ± 4	597^{+79}_{-65}	> 316	Yes	2.33	35.62	0	0	1	✓
K01615.01	Kepler-908 b	5670	7.88	67 ± 4	602^{+77}_{-65}	1317^{+1607}_{-724}	Yes	1.36	1.34	0	4608	1	
K02022.01	Kepler-349 b	5756	7.71	64 ± 6	617^{+103}_{-72}	1686^{+2185}_{-976}	Yes	1.99	5.93	0	0	1	✓✓
K02022.02	Kepler-349 c	5756	7.71	64 ± 6	617^{+103}_{-72}	1686^{+2185}_{-976}	Yes	1.97	12.25	0	0	1	✓✓
K00620.01	Kepler-51 b	5635	8.14	48 ± 8	623^{+75}_{-65}	> 258	Yes	6.62	45.16	0	0	1	✓
K00620.03	Kepler-51 c	5635	8.14	48 ± 8	623^{+75}_{-65}	> 258	Yes	5.49	85.32	4	0	1	
K00620.02	Kepler-51 d	5635	8.14	48 ± 8	623^{+75}_{-65}	> 258	Yes	9.04	130.18	0	0	1	✓
K02803.01	Kepler-1877 b	5506	8.37	3 ± 12	624^{+69}_{-65}	> 726	Maybe	0.55	2.38	0	1024	1	
K00720.04	Kepler-221 b	5070	9.3	21 ± 5	636^{+120}_{-115}	> 341	Yes	1.51	2.8	0	0	1	✓
K00720.01	Kepler-221 c	5070	9.3	21 ± 5	636^{+120}_{-115}	> 341	Yes	2.86	5.69	0	0	1	✓
K00720.02	Kepler-221 d	5070	9.3	21 ± 5	636^{+120}_{-115}	> 341	Yes	2.57	10.04	0	0	1	✓
K00720.03	Kepler-221 e	5070	9.3	21 ± 5	636^{+120}_{-115}	> 341	Yes	2.58	18.37	4	0	1	
K03097.02	Kepler-431 b	6259	16.16	80 ± 3	–	671^{+1092}_{-458}	–	0.93	6.8	4	4103	1	
K03097.03	Kepler-431 c	6259	16.16	80 ± 3	–	671^{+1092}_{-458}	–	0.93	8.7	4	4103	1	
K03097.01	Kepler-431 d	6259	16.16	80 ± 3	–	671^{+1092}_{-458}	–	1.08	11.92	4	4103	1	
K01982.01	Kepler-1781 b	5363	9.17	–	708^{+80}_{-78}	–	–	1.95	4.89	0	0	0	
K03375.01	Kepler-1918 b	5522	9.11	–	722^{+75}_{-71}	–	–	2.19	47.06	0	0	0	
K01835.02	Kepler-326 b	5142	9.56	8 ± 8	724^{+108}_{-103}	> 506	Yes	1.25	2.25	0	1664	1	
K01835.01	Kepler-326 c	5142	9.56	8 ± 8	724^{+108}_{-103}	> 506	Yes	1.38	4.58	0	1664	1	
K01835.03	Kepler-326 d	5142	9.56	8 ± 8	724^{+108}_{-103}	> 506	Yes	1.31	6.77	0	1664	1	
K01797.01	Kepler-954 b	4736	10.68	4 ± 11	727^{+222}_{-184}	> 270	Yes	2.16	16.78	0	1024	1	
K01821.01	Kepler-963 b	5383	9.42	–	748^{+80}_{-78}	–	–	2.64	9.98	0	0	0	
K03681.01	Kepler-1514 b	5852	7.87	69 ± 2	758^{+416}_{-142}	1302^{+1622}_{-754}	Yes	11.94	217.83	0	1540	1	
K03681.02	Kepler-1514 c	5852	7.87	69 ± 2	758^{+416}_{-142}	1302^{+1622}_{-754}	Yes	1.17	10.51	4	1540	1	
K00647.01	Kepler-634 b	6272	–	77 ± 3	–	768^{+1250}_{-527}	–	2.13	5.17	0	7	1	
K02037.01	Kepler-1995 b	4746	10.8	9 ± 21	772^{+213}_{-194}	> 223	Yes	3.46	73.76	0	4096	1	✓
K01781.02	Kepler-411 b	4920	10.32	4 ± 3	775^{+164}_{-166}	> 396	Yes	2.2	3.01	4	0	1	
K01781.01	Kepler-411 c	4920	10.32	4 ± 3	775^{+164}_{-166}	> 396	Yes	3.47	7.83	0	0	1	✓
K07375.01	–	4212	3.88	117 ± 9	104^{+235}_{-72}	70^{+37}_{-21}	Yes	1.73	4.85	0	2560	1	
K03991.01	–	5226	5.22	98 ± 3	71^{+91}_{-48}	354^{+253}_{-145}	Maybe	1.37	1.57	0	2176	1	
K01546.01	–	5639	0.9	33 ± 24	75^{+134}_{-51}	> 316	Maybe	11.92	0.92	0	2176	1	
K05482.01	–	5519	0.81	–	77^{+144}_{-53}	–	–	2.96	31.71	4	2690	0	
K00064.01	–	5306	2.23	3 ± 4	81^{+129}_{-55}	> 567	No	10.49	1.95	4	4614	1	
K06188.01	–	5209	1.62	6 ± 11	84^{+171}_{-58}	> 554	Maybe	2.75	1.65	0	2048	1	
K02695.01	–	5174	2.88	–	86^{+176}_{-59}	–	–	20.23	2.5	4	640	0	
K07449.01	–	4928	1.31	–	92^{+194}_{-63}	–	–	20.43	1.32	4	2048	0	
K06130.01	–	4560	3.02	-1 ± 25	94^{+217}_{-65}	> 186	Yes	1.45	1.54	0	2976	1	
K06195.01	–	4677	1.42	-8 ± 30	94^{+210}_{-65}	> 208	Yes	2.28	1.44	0	2048	1	

NOTE— EW^{*}_{Li} is the lithium equivalent width *after* subtracting a constant 7.5 mÅ to account for the Fe I 6707.44 Å blend (see Section 2.3). Two checkmarks (✓✓) denote confirmed planets with two-sided t_{gyro} and t_{Li} for which both the age and the planet are expected to be reliable. One checkmark (✓) denotes confirmed planets with two-sided t_{gyro} only. "Confirmed" planets appear in the machine-readable version before"candidate" planets. Planetary sizes are mostly drawn from (in order of precedence) Petigura et al. (2022), Berger et al. (2020a), and Thompson et al. (2018), and might be unphysical for grazing planets. The bit quality flags for the rotation-based ages, Q_{star}, are described in Section 4.1. Concisely summarized, they are: Bit 0: $T_{eff}/K \in [3800-6200]$? Bit 1: $\log g$<4.2? Bit 2: M_G<3.9 or $M_G > 8.5$? Bit 3: In KEBC? Bit 4: Large $d_{xm,Kep-Gaia}$? Bit 5: Confused Kep-Gaia crossmatch? Bit 6: Gaia DR3 non-single star? Bit 7: RUWE>1.4? Bit 8: Crowded? Bit 9: Far from main sequence? Bit 10: Spectroscopic |[Fe/H]|>0.3? Bit 11: S21 CP/CB? Bit 12: P_{rot} not in the homogeneous S19 S21 sample? As an example, Kepler-1627 has Q_{star} flagged with bit 11 and bit 7. The analogous planet quality bitmask, Q_{planet}, has the following meaning. Bit 0: Candidate not reliable? Bit 1: MES<10? Bit 2: Grazing? For a star to have a high likelihood of being "reliable for gyrochronology" we suggest a Q_{star} bitmask with bits 0–10 not raised, and for a planet to be "reliable", we suggest Q_{planet} to be zero.

Table 2. Ages of Kepler target stars derived from rotation periods. The full machine-readable table includes 37,892 stars with finite reported gyrochrone ages. The quality bitmask is as in Table 1; requiring bits zero to ten to be null yields 23,813 stars for which gyrochronology is likely to be valid.

KIC	Gaia DR3	$T_{\rm eff}$	$P_{\rm rot}$	$t_{\rm gyro}$	$Q_{\rm star}$
–	–	K	days	Myr	int
8367679	2126373303927600000	5980	7.44	1062^{+815}_{-369}	0
11954016	2133663925009149952	5423	24.88	3230^{+330}_{-301}	0
1865152	2051034045638265984	5878	7.67	879^{+891}_{-274}	0
4447913	2100652256617096832	4654	35.67	> 4000	0
11085139	2129657064120722688	5507	20.49	2596^{+322}_{-267}	0

REFERENCES

Aigrain, S., Llama, J., Ceillier, T., et al. 2015, MNRAS, 450, 3211

Akeson, R. L., Chen, X., Ciardi, D., et al. 2013, PASP, 125, 989

Alzate, J. A., Bruzual, G., & Díaz-González, D. J. 2021, MNRAS, 501, 302

Amard, L., & Matt, S. P. 2020, ApJ, 889, 108

Amard, L., Palacios, A., Charbonnel, C., et al. 2019, A&A, 631, A77

Amard, L., Roquette, J., & Matt, S. P. 2020, MNRAS, 499, 3481

Angus, R., Aigrain, S., Foreman-Mackey, D., & McQuillan, A. 2015, MNRAS, 450, 1787

Angus, R., Morton, T., Aigrain, S., Foreman-Mackey, D., & Rajpaul, V. 2018, MNRAS, 474, 2094

Angus, R., Morton, T. D., Foreman-Mackey, D., et al. 2019, AJ, 158, 173

Anthropic. 2024, Claude, v3, Anthropic, Conversational AI model used for editing manuscript and generating testable code; the authors wrote all of the original manuscript text. https://claude.ai/

Barber, M. G., Mann, A. W., Bush, J. L., et al. 2022, AJ, 164, 88

Barnes, S. A. 2003, ApJ, 586, 464

Barnes, S. A., Weingrill, J., Fritzewski, D., Strassmeier, K. G., & Platais, I. 2016, ApJ, 823, 16

Berger, T. A., Howard, A. W., & Boesgaard, A. M. 2018, ApJ, 855, 115

Berger, T. A., Huber, D., Gaidos, E., van Saders, J. L., & Weiss, L. M. 2020a, AJ, 160, 108

Berger, T. A., Huber, D., van Saders, J. L., et al. 2020b, AJ, 159, 280

Binney, J., Dehnen, W., & Bertelli, G. 2000, MNRAS, 318, 658

Bonomo, A. S., Sozzetti, A., Lovis, C., et al. 2014, A&A, 572, A2

Borucki, W. J., Koch, D., Basri, G., et al. 2010, Science, 327, 977

Bouma, L. G., Curtis, J. L., Hartman, J. D., Winn, J. N., & Bakos, G. Á. 2021, AJ, 162, 197

Bouma, L. G., Palumbo, E. K., & Hillenbrand, L. A. 2023, ApJL, 947, L3

Bouma, L. G., Hartman, J. D., Brahm, R., et al. 2020, AJ, 160, 239

Bouma, L. G., Curtis, J. L., Masuda, K., et al. 2022a, AJ, 163, 121

Bouma, L. G., Kerr, R., Curtis, J. L., et al. 2022b, AJ, 164, 215

Boyle, A. W., & Bouma, L. G. 2023, AJ, 166, 14

Cantat-Gaudin, T., Jordi, C., Vallenari, A., et al. 2018, A&A, 618, A93

Cantat-Gaudin, T., Anders, F., Castro-Ginard, A., et al. 2020, A&A, 640, A1

Capistrant, B. K., Soares-Furtado, M., Vanderburg, A., et al. 2024, AJ, 167, 54

Carlos, M., Meléndez, J., Spina, L., et al. 2019, MNRAS, 485, 4052

Castro-Ginard, A., Jordi, C., Luri, X., et al. 2018, A&A, 618, A59

Chaboyer, B., Demarque, P., & Pinsonneault, M. H. 1995, ApJ, 441, 865

Chiti, F., van Saders, J. L., Heintz, T. M., et al. 2024, arXiv e-prints, arXiv:2403.12129

Choi, J., Dotter, A., Conroy, C., et al. 2016, ApJ, 823, 102

Christiansen, J. L., Zink, J. K., Hardegree-Ullman, K. K., et al. 2023, AJ, 166, 248

Claytor, Z. R., van Saders, J. L., Santos, Â. R. G., et al. 2020, ApJ, 888, 43

Curtis, J. 2024, in American Astronomical Society Meeting Abstracts, Vol. 243, American Astronomical Society Meeting Abstracts, 458.08

Curtis, J. L., Agüeros, M. A., Douglas, S. T., & Meibom, S. 2019, ApJ, 879, 49

Curtis, J. L., Vanderburg, A., Torres, G., et al. 2018, AJ, 155, 173
Curtis, J. L., Agüeros, M. A., Matt, S. P., et al. 2020, ApJ, 904, 140
David, T. J., Angus, R., Curtis, J. L., et al. 2022, ApJ, 933, 114
David, T. J., Petigura, E. A., Luger, R., et al. 2019, ApJL, 885, L12
David, T. J., Contardo, G., Sandoval, A., et al. 2021, AJ, 161, 265
Denissenkov, P. A., Pinsonneault, M., Terndrup, D. M., & Newsham, G. 2010, ApJ, 716, 1269
Dotter, A. 2016, ApJS, 222, 8
Dungee, R., van Saders, J., Gaidos, E., et al. 2022, ApJ, 938, 118
Engle, S. G. 2024, ApJ, 960, 62
Engle, S. G., & Guinan, E. F. 2023, ApJL, 954, L50
Epstein, C. R., & Pinsonneault, M. H. 2014, ApJ, 780, 159
Fortney, J. J., Marley, M. S., & Barnes, J. W. 2007, ApJ, 659, 1661
Fritzewski, D. J., Barnes, S. A., James, D. J., & Strassmeier, K. G. 2021, A&A, 652, A60
Fritzewski, D. J., Van Reeth, T., Aerts, C., et al. 2024, A&A, 681, A13
Fulton, B. J., & Petigura, E. A. 2018, AJ, 156, 264
Fulton, B. J., Petigura, E. A., Howard, A. W., et al. 2017, AJ, 154, 109
Gaia Collaboration, Babusiaux, C., van Leeuwen, F., et al. 2018, A&A, 616, A10
Gaia Collaboration, Vallenari, A., Brown, A. G. A., et al. 2022, arXiv e-prints, arXiv:2208.00211
Gallet, F., & Bouvier, J. 2015, A&A, 577, A98
Ge, J., Zhang, H., Zang, W., et al. 2022, arXiv e-prints, arXiv:2206.06693
Gilbert, G. J. 2022, AJ, 163, 111
Gillen, E., Briegal, J. T., Hodgkin, S. T., et al. 2020, MNRAS, 492, 1008
Green, G. M., Schlafly, E., Zucker, C., Speagle, J. S., & Finkbeiner, D. 2019, ApJ, 887, 93
Greiss, S., Steeghs, D., Gänsicke, B. T., et al. 2012, AJ, 144, 24
Gruner, D., Barnes, S. A., & Weingrill, J. 2023, A&A, 672, A159
Gupta, A., & Schlichting, H. E. 2019, MNRAS, 487, 24
Heavens, A., Panter, B., Jimenez, R., & Dunlop, J. 2004, Nature, 428, 625
Hedges, C., Hughes, A., Zhou, G., et al. 2021, AJ, 162, 54
Herschel, J. F. W. 1864, Philosophical Transactions of the Royal Society of London Series I, 154, 1
Hopkins, A. M., & Beacom, J. F. 2006, ApJ, 651, 142
Huber, D., Chaplin, W. J., Christensen-Dalsgaard, J., et al. 2013, ApJ, 767, 127
Huber, D., Zinn, J., Bojsen-Hansen, M., et al. 2017, ApJ, 844, 102
Hunter, J. D., et al. 2007, Computing in science and engineering, 9, 90
Isern, J. 2019, ApJL, 878, L11
Izidoro, A., Ogihara, M., Raymond, S. N., et al. 2017, MNRAS, 470, 1750
Jeffries, R. D., Jackson, R. J., Wright, N. J., et al. 2023, MNRAS, 523, 802
Jenkins, J. M., Caldwell, D. A., & Borucki, W. J. 2002, ApJ, 564, 495
Johnson, J. A., Petigura, E. A., Fulton, B. J., et al. 2017, AJ, 154, 108
Kawaler, S. D. 1989, ApJL, 343, L65
Keppler, M., Benisty, M., Müller, A., et al. 2018, A&A, 617, A44
Kerr, R. M. P., Rizzuto, A. C., Kraus, A. L., & Offner, S. S. R. 2021, ApJ, 917, 23
Kipping, D., & Bakos, G. 2011, ApJ, 733, 36
Kirk, B., Conroy, K., Prša, A., et al. 2016, AJ, 151, 68
Klein, B., Zicher, N., Kavanagh, R. D., et al. 2022, MNRAS, 512, 5067
Kolbl, R., Marcy, G. W., Isaacson, H., & Howard, A. W. 2015, AJ, 149, 18
Kounkel, M., & Covey, K. 2019, AJ, 158, 122
Kounkel, M., Covey, K., & Stassun, K. G. 2020, AJ, 160, 279
Livingston, J. H., Dai, F., Hirano, T., et al. 2018, AJ, 155, 115
Lu, Y., Angus, R., Foreman-Mackey, D., & Hattori, S. 2024, AJ, 167, 159
Lu, Y. L., Angus, R., Curtis, J. L., David, T. J., & Kiman, R. 2021, AJ, 161, 189
Lu, Y. L., Curtis, J. L., Angus, R., David, T. J., & Hattori, S. 2022, AJ, 164, 251
Mamajek, E. E., & Hillenbrand, L. A. 2008, ApJ, 687, 1264
Mann, A. W., Gaidos, E., Mace, G. N., et al. 2016, ApJ, 818
Marois, C., Macintosh, B., Barman, T., et al. 2008, Science, 322, 1348
Masuda, K. 2014, ApJ, 783, 53
—. 2022a, ApJ, 937, 94
—. 2022b, ApJ, 933, 195
Masuda, K., Petigura, E. A., & Hall, O. J. 2022, MNRAS, 510, 5623
Mathur, S., Huber, D., Batalha, N. M., et al. 2017, ApJS, 229, 30
Mathur, S., Claytor, Z. R., Santos, Â. R. G., et al. 2023, ApJ, 952, 131
Matt, S. P., Brun, A. S., Baraffe, I., Bouvier, J., & Chabrier, G. 2015, ApJL, 799, L23
Mazeh, T., Perets, H. B., McQuillan, A., & Goldstein, E. S. 2015, ApJ, 801, 3
McQuillan, A., Mazeh, T., & Aigrain, S. 2013, ApJL, 775, L11
—. 2014, ApJS, 211, 24
Meibom, S., Barnes, S. A., Platais, I., et al. 2015, Nature, 517, 589
Meibom, S., Mathieu, R. D., & Stassun, K. G. 2007, ApJL, 665, L155
Meibom, S., Torres, G., Fressin, F., et al. 2013, Nature, 499, 55
Mills, S. M., & Fabrycky, D. C. 2017, AJ, 153, 45
Miyazaki, S., & Masuda, K. 2023, AJ, 166, 209

Mor, R., Robin, A. C., Figueras, F., Roca-Fàbrega, S., & Luri, X. 2019, A&A, 624, L1
Morton, T. D., Bryson, S. T., Coughlin, J. L., et al. 2016, ApJ, 822, 86
Nardiello, D., Malavolta, L., Desidera, S., et al. 2022, A&A, 664, A163
Newton, E. R., Irwin, J., Charbonneau, D., et al. 2016, ApJ, 821, 93
Newton, E. R., Mann, A. W., Kraus, A. L., et al. 2021, AJ, 161, 65
Nordström, B., Mayor, M., Andersen, J., et al. 2004, A&A, 418, 989
Noyes, R. W., Hartmann, L. W., Baliunas, S. L., Duncan, D. K., & Vaughan, A. H. 1984, ApJ, 279, 763
O'Donovan, F. T., Charbonneau, D., Mandushev, G., et al. 2006, ApJL, 651, L61
Owen, J. E. 2019, Annual Review of Earth and Planetary Sciences, 47, 67
Owen, J. E., & Lai, D. 2018, MNRAS, 479, 5012
Pecaut, M. J., & Mamajek, E. E. 2013, ApJS, 208, 9
Petigura, E. A., Howard, A. W., Marcy, G. W., et al. 2017, AJ, 154, 107
Petigura, E. A., Marcy, G. W., Winn, J. N., et al. 2018, AJ, 155, 89
Petigura, E. A., Rogers, J. G., Isaacson, H., et al. 2022, AJ, 163, 179
Plavchan, P., Barclay, T., Gagné, J., et al. 2020, Nature, 582, 497
Price-Whelan, A. M., Sipőcz, B. M., Günther, H. M., et al. 2018, AJ, 156, 123
Quinn, S. N., White, R. J., Latham, D. W., et al. 2012, ApJL, 756, L33
Rampalli, R., Agüeros, M. A., Curtis, J. L., et al. 2021, ApJ, 921, 167
Rauer, H., Catala, C., Aerts, C., et al. 2014, Experimental Astronomy, 38, 249
Raymond, S. N., Kokubo, E., Morbidelli, A., Morishima, R., & Walsh, K. J. 2014, in Protostars and Planets VI, ed. H. Beuther, R. S. Klessen, C. P. Dullemond, & T. Henning, 595–618
Rebull, L. M., Stauffer, J. R., Hillenbrand, L. A., et al. 2022, AJ, 164, 80
Rebull, L. M., Stauffer, J. R., Bouvier, J., et al. 2016, AJ, 152, 114
Reinhold, T., Bell, K. J., Kuszlewicz, J., Hekker, S., & Shapiro, A. I. 2019, A&A, 621, A21
Reinhold, T., & Gizon, L. 2015, A&A, 583, A65
Reinhold, T., Shapiro, A. I., Solanki, S. K., & Basri, G. 2023, A&A, 678, A24
Ricker, G. R., Winn, J. N., Vanderspek, R., et al. 2015, Journal of Astronomical Telescopes, Instruments, and Systems, 1, 014003
Rizzuto, A. C., Newton, E. R., Mann, A. W., et al. 2020, AJ, 160, 33
Rogers, J. G., & Owen, J. E. 2021, MNRAS, 503, 1526
Ruiz-Lara, T., Gallart, C., Bernard, E. J., & Cassisi, S. 2020, Nature Astronomy, 4, 965
Sandoval, A., Contardo, G., & David, T. J. 2021, ApJ, 911, 117
Santos, A. R. G., Breton, S. N., Mathur, S., & García, R. A. 2021, ApJS, 255, 17
Santos, A. R. G., García, R. A., Mathur, S., et al. 2019, ApJS, 244, 21
Saunders, N., van Saders, J. L., Lyttle, A. J., et al. 2024, ApJ, 962, 138
See, V., Yuxi, Lu, Amard, L., & Roquette, J. 2024, arXiv e-prints, arXiv:2405.00779
Sestito, P., & Randich, S. 2005, A&A, 442, 615
Silva Aguirre, V., Bojsen-Hansen, M., Slumstrup, D., et al. 2018, MNRAS, 475, 5487
Skrutskie, M. F., Cutri, R. M., Stiening, R., et al. 2006, AJ, 131, 1163
Skumanich, A. 1972, ApJ, 171, 565
Soderblom, D. R. 2010, ARA&A, 48, 581
Southworth, J. 2011, MNRAS, 417, 2166
Sozzetti, A., Torres, G., Charbonneau, D., et al. 2007, ApJ, 664, 1190
Spada, F., & Lanzafame, A. C. 2020, A&A, 636, A76
Thompson, S. E., Coughlin, J. L., Hoffman, K., et al. 2018, ApJS, 235, 38
Tofflemire, B. M., Rizzuto, A. C., Newton, E. R., et al. 2021, AJ, 161, 171
Tran, Q. H., Bowler, B. P., Cochran, W. D., et al. 2024, AJ, 167, 193
Vach, S., Zhou, G., Huang, C. X., et al. 2024, arXiv e-prints, arXiv:2403.03261
Van Der Walt, S., Colbert, S. C., & Varoquaux, G. 2011, Computing in Science & Engineering, 13, 22
Van Eylen, V., Agentoft, C., Lundkvist, M. S., et al. 2018, MNRAS, 479, 4786
van Saders, J. L., Ceillier, T., Metcalfe, T. S., et al. 2016, Nature, 529, 181
Vidotto, A. A., Gregory, S. G., Jardine, M., et al. 2014, MNRAS, 441, 2361
Virtanen, P., Gommers, R., Oliphant, T. E., et al. 2020, Nature Methods, 17, 261
Vogt, S. S., Allen, S. L., Bigelow, B. C., et al. 1994a, SPIE Conference Series, ed. D. L. Crawford & E. R. Craine, Vol. 2198
Vogt, S. S., Allen, S. L., Bigelow, B. C., et al. 1994b, in Society of Photo-Optical Instrumentation Engineers (SPIE) Conference Series, Vol. 2198, Society of Photo-Optical Instrumentation Engineers (SPIE) Conference Series, ed. D. L. Crawford & E. R. Craine, 362
Walkowicz, L. M., & Basri, G. S. 2013, MNRAS, 436, 1883
Wilson, R. F., Barclay, T., Powell, B. P., et al. 2023, ApJS, 269, 5
Winn, J. N., Johnson, J. A., Narita, N., et al. 2008, ApJ, 682, 1283
Wood, M. L., Mann, A. W., Barber, M. G., et al. 2023, AJ, 165, 85
Xiang, M., & Rix, H.-W. 2022, Nature, 603, 599

York, D. G., Adelman, J., Anderson, John E., J., et al. 2000, AJ, 120, 1579

Zakhozhay, O. V., Launhardt, R., Trifonov, T., et al. 2022, A&A, 667, L14

Zari, E., Hashemi, H., Brown, A. G. A., Jardine, K., & de Zeeuw, P. T. 2018, A&A, 620, A172

Zhou, G., Wirth, C. P., Huang, C. X., et al. 2022, AJ, 163, 289

Ziegler, C., Law, N. M., Morton, T., et al. 2017, AJ, 153, 66

Zong, W., Fu, J.-N., De Cat, P., et al. 2018, ApJS, 238, 30

APPENDIX

A. ROTATION PERIOD CATALOG COMPARISON

While we opted for the S19 and S21 rotation period catalogs, the analysis by Reinhold et al. (2023) bears comment. Reinhold et al. (2023) used a similar selection function as Santos et al. (all Kepler stars), and considered a novel period measurement approach based on the gradient of the power spectrum (GPS). Their method likely provides greater completeness, due to its greater sensitivity to signals that are only weakly periodic.

Figure 8 shows histograms of the differences between reported periods from these various studies. The left panel compares overlapping stars from McQuillan et al. (2014) and the Santos et al. studies. The periods agree at a precision of $\lesssim 0.01 P_{\rm rot}$ for $P_{\rm rot} \lesssim 15$ days, and at $\lesssim 0.03 P_{\rm rot}$ for $P_{\rm rot} \approx 30$ days. A small bias exists at $P_{\rm rot} \approx 10$ days, in the sense that the Santos periods tend to be $\approx 1\%$ faster for such stars.

The right panel compares overlapping periods from the Reinhold et al. (2023) GPS method and the Santos et al. studies. The periods agree at a precision of $\lesssim 0.20 P_{\rm rot}$ for $P_{\rm rot} \lesssim 15$ days, and at $\lesssim 0.30 P_{\rm rot}$ for $P_{\rm rot} \approx 30$ days. A bias develops past $P_{\rm rot} \gtrsim 30$ days, in the sense that the Santos et al. periods tend to be 10-20% longer than the GPS periods. The origin of this larger scatter could be connected to the need for the GPS method to determine the "α calibration factor", which is known only at a statistical level for large stellar populations (see Reinhold et al. 2023). While we considered deriving independent rotation-based ages using the Reinhold et al. (2023) GPS periods with an inflated empirical uncertainty, we ultimately opted against this path. A rotation period difference of 20-30% away from the "true period" could sufficiently skew a star's age that we prefer to restrict our attention to the stars for which precision is a possible outcome.

B. DEFINING AN "ISOCHRONALLY FAR FROM THE MAIN SEQUENCE" BOUNDARY

The (arbitrary) method used to construct the orange line in the lower panel of Figure 1 was as follows. The line is defined as the maximum of two numerically-determined functions, $f_0(T_{\rm eff})$ and $f_1(T_{\rm eff})$. We defined f_0 by fitting an $N^{\rm th}$-order polynomial to the stars with rotation periods for which $t_{\rm B20,iso}/(+\sigma_{t,\rm B20,iso}) \approx 3$ and $T_{\rm eff} \in [3700, 5900]$ K, where $t_{\rm B20,iso}$ was the isochronal age reported by Berger et al. (2020b). We let the order of the fit vary from N=1 to 10, minimized the Bayesian Information Criterion, and found N=6. By eye, this yielded a plausible locus for $T_{\rm eff} \lesssim 5300$ K. However, for F and G dwarfs, the resulting locus allowed for stars that were "too evolved"; the density of KOIs was anomalously low in this region of the $\log g$ vs. $T_{\rm eff}$ plane. We therefore visually selected KOIs that appeared to be near the main sequence – i.e. most of the yellow points in Figure 1 – and used them to fit a separate polynomial f_1 through a similar BIC-minimization procedure, which yielded N=3. This polynomial, f_1, is shown in very faint opacity in Figure 1. The portion of the orange locus from $\approx$5300–6200 K is set as $f_1 + c$, for c a constant offset that we defined to be 0.1 dex above the "KOI main sequence". The exact break-point in temperature is automatically set by

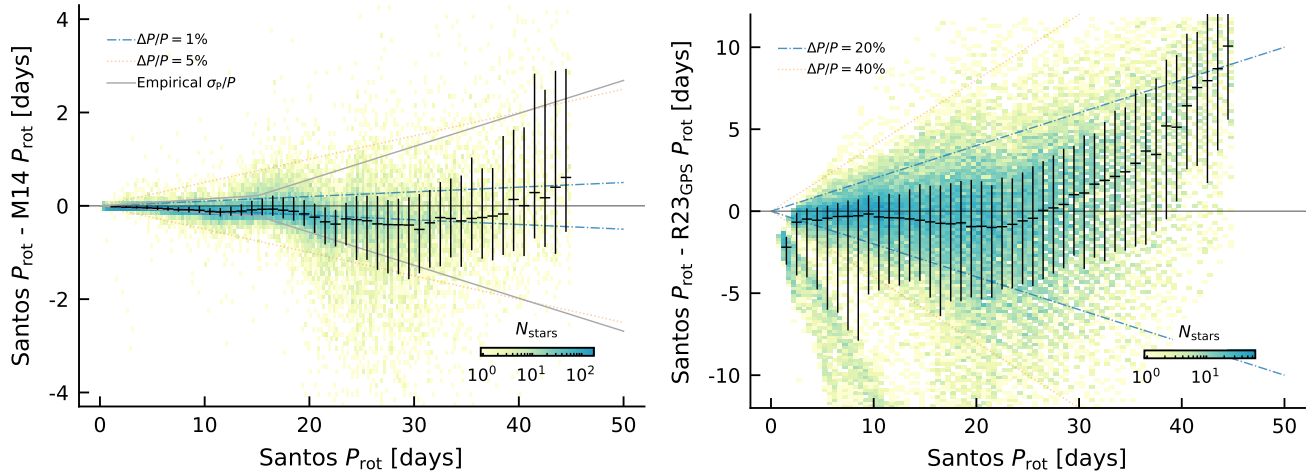

Figure 8. Comparison of reported literature stellar rotation periods. "Santos" refers to the concatenation of Santos et al. (2019) and Santos et al. (2021). "M14" refers to McQuillan et al. (2014). "R23$_{\rm GPS}$" refers to the Gradient of Power Spectrum periods from Reinhold et al. (2023). The background is a 2-D histogram with a logarithmic color stretch that counts overlapping stars between these studies. The black errorbars show the median and $\pm 1\sigma$ range of period the differences in 1-day bins. The solid gray "empirical $\sigma_{\rm P}/P$" line in the left panel shows the expected $\pm 1\sigma$ range that would be spanned if the independent $P_{\rm rot}$ measurements had gaussian uncertainties drawn following the empirical estimate described in Section 2.1. Note the different vertical scales.

$\max(f_0, f_1 + c)$. While we do report rotation-based ages for stars above this orange locus, they are flagged as not being near the main sequence in the $\log g$ vs. $T_{\rm eff}$ plane.

C. CASES WITH "INCONSISTENT" ROTATION AND LITHIUM-BASED AGES

In this section we discuss the systems with confirmed planets that have nominally discrepant rotation and lithium-based ages. We find that only one of them, Kepler-786, is interesting.

Kepler-1 ——TrES-2/Kepler-1 (O'Donovan et al. 2006) is a ≈2.5 day near-grazing hot Jupiter orbiting a G0 V primary which has been studied in detail by multiple investigators (e.g. Sozzetti et al. 2007; Winn et al. 2008; Kipping & Bakos 2011; Southworth 2011). Our lithium-based age of this system (785^{+845}_{-419} Myr), derived from $\mathrm{EW}^{*}_{\rm Li}$=81±3 mÅ, qualitatively agrees with the previously noted lithium abundance (Sozzetti et al. 2007). However, we detect no photometric rotation signal, and the spectroscopic $v \sin i$ is low. The lithium age is strongly asymmetric because of the scatter in $\mathrm{EW}_{\rm Li}$ vs. $T_{\rm eff}$ over ages $t \gtrsim 1$ Gyr for early G dwarfs. We calculate a 2σ upper limit on $t_{\rm Li}$ of 2.8 Gyr, and a 3σ upper limit of 6.1 Gyr. The non-detection of rotation, while mildly surprising, is not shocking if the system's true age is in this long tail.

Kepler-101 ——This ≈5500 K star has $\mathrm{EW}^{*}_{\rm Li}$=100±5 mÅ, nominally implying $t_{\rm Li}$≈200-800 Myr, but no rotation detection. Our automated flags noted that this star has a low surface gravity, high luminosity, and is far from the main sequence. Bonomo et al. (2014) concur: this star is a sub-giant slightly more massive than the Sun; no rotation detection is expected; the lithium likely simply survived over the star's main sequence lifetime.

Kepler-108 ——This system of two mutually inclined giant planets (Mills & Fabrycky 2017) has a $T_{\rm eff}$≈5600 K host star with a strong lithium detection, and no rotation detection. The host star is entering the red giant branch; this has been previously noted through asteroseismology (Huber et al. 2013), and our analysis of the Keck/HIRES spectrum with `SpecMatch-Synth` (Petigura et al. 2017) concurs, yielding $T_{\rm eff}$=5668±100 K, $\log g$=3.8±0.1, [Fe/H]=0.38±0.06, and $v \sin i$=3.2±1.0km s^{-1}. Given the star's high mass, the high lithium content and lack of rotation detection is not surprising.

Kepler-786 ——This K3 V star has a surprisingly high lithium content. The spectrum is single-lined, with `SpecMatch-Synth` derived parameters of $T_{\rm eff}$=4769±100 K, $\log g$=4.5±0.1, [Fe/H]=0.11±0.06, and $v \sin i$=2.4±0.6km s^{-1}. Yet with $\mathrm{EW}^{*}_{\rm Li}$=83±6 mÅ, the lithium age of 228^{+168}_{-87} Myr would predict an obvious rotation signal. None is present in the Kepler light curve, consistent with the low $v \sin i$. Out of all "apparently discrepant" lithium and rotation measurements discussed in this appendix, this is the only one that seems to remain discrepant after scrutiny. The Ca II doublet is in emission, with $R'_{\rm HK} = -4.7 \pm 0.5$, which suggests an age at least as old as the Hyades (Mamajek & Hillenbrand 2008). The Balmer lines are in absorption, and display no obvious signatures of youth.

Kepler-1644 ——The rotation-based age of this system (77^{+144}_{-53} Myr) is nominally much lower than the lithium limit (>767 Myr). The Kepler light curve shows a ≈1% amplitude 1.4 day rotation signal with many flares. However the automated quality flags note that the star has low (photometric) surface gravity, a high RUWE ($\mathrm{RUWE}_{\rm DR3}$=7.0), and that it is far from the main sequence. The Keck/HIRES spectrum also shows visually narrow lines, with a `SpecMatch-Synth` $v \sin i \leq 2$km s^{-1}. However, we performed a cross-correlation between the HIRES spectrum and the nearest matches in the Keck/HIRES template library (Kolbl et al. 2015), and found that on 31 July 2022 (UT) the system displayed a broad CCF with a blended second component at ≈+26 km s^{-1} relative to the primary, with a best-fit flux-ratio of ≈3.4%, and a preferred $T_{\rm eff,B}$≈4400 K. The spectrum and astrometric excess noise therefore point to this system being an unresolved binary, which calls the reliability of the rotation-based age into question. The non-detection of the companion from Robo-AO imaging at Palomar (Ziegler et al. 2017) suggests that the companion(s) are likely within $\rho \lesssim 0.3''$.

Kepler-1699 ——This system is in a similar qualitative regime as Kepler-1644, with an apparently young $t_{\rm gyro}$=85^{+106}_{-58} Myr derived from a ≈2% amplitude 4.2 day rotation signal, and no evidence for lithium. The system has $\mathrm{RUWE}_{\rm DR3}$=19.1. From the same style of CCF analysis from the Keck/HIRES spectrum acquired on 31 Aug 2022 (UT), we also find a double-peaked CCF, in this case with a secondary component at ≈−16 km s^{-1} relative to the primary with $T_{\rm eff,B}$≈4900 K. This putative companion is similarly not detected in high-resolution imaging (Ziegler et al. 2017). The rotation-based age is questionable, given that we do not know which source the rotation signal is from, or whether the stars have interacted.

Kepler-1943 ——This system nominally has a 409^{+520}_{-254} Myr lithium age, and no reported rotation detection. However, the star is flagged as being over-luminous, low-surface gravity, and far from the main sequence. In other words, it is a subgiant.

Kepler-639, Kepler-320, Kepler-1719, Kepler-1876, Kepler-1072, Kepler-1743, Kepler-1929, Kepler-1488 ——These eight systems all have nominally two-sided lithium age posteriors between 1 and 3 Gyr, and yet lack rotation period detections. All are subgiants, flagged with $Q_{\rm star}$ under various combinations of bits 1, 2, and 9.

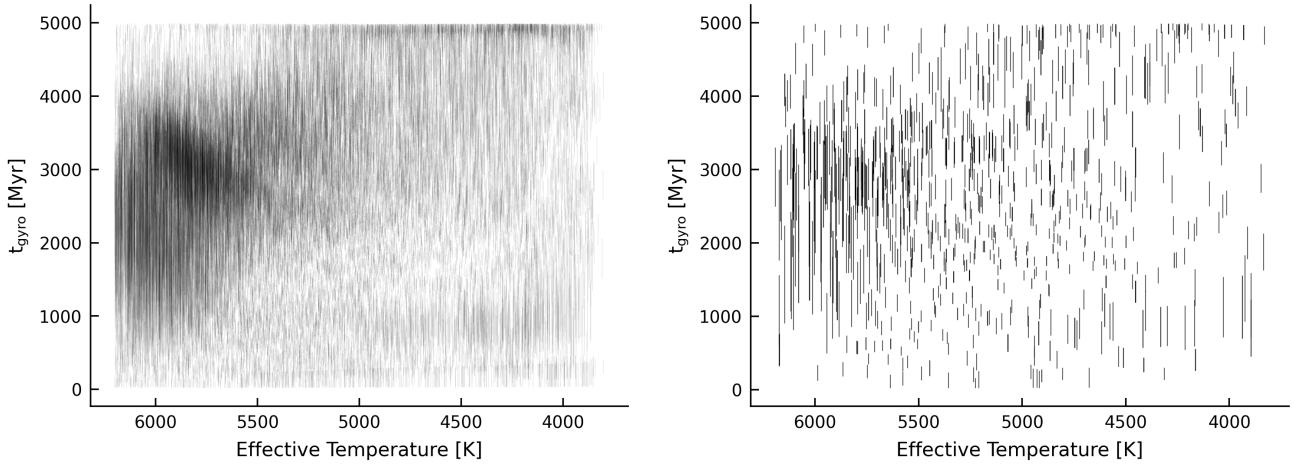

Figure 9. Rotation-based age vs. effective temperature. The entire Kepler sample is shown on the left. KOI hosts are shown on the right. Each bar shows the $\pm 1\sigma$ uncertainty for a star's age as derived from its rotation period. Notable features are discussed in Appendix D.

D. AGE DIAGNOSTICS

Figure 9 is a visualization of $t_{\rm gyro}$ vs. $T_{\rm eff}$ for our rotation-based age catalog. Each bar denotes the $\pm 1\sigma$ uncertainty for a star's rotation-based age: this plot can be viewed as the transformation of the left panel of Figure 2. The overdensity of $P_{\rm rot} \approx 20$ day G dwarfs corresponds to the large overdensity at $t_{\rm gyro} \approx 3$ Gyr. The (non-physical) deficit of $\sim$22 day rotators appears as a deficit between 5500–6000 K. A second deficit is also visible from 3800–5000 K; it is associated with the "intermediate period gap", which may be associated with a transition from spot-dominated to faculae-dominated light curves (e.g. Reinhold et al. 2019), or with rapid spin-down at Rossby numbers near 0.5 (Lu et al. 2022). At $\approx$1 Gyr, stalled spin-down yields larger uncertainties for K dwarfs. The pile-up near $\approx$5 Gyr is imposed by our choice of prior; given that `gyro-interp` returns non-calibrated ages in this regime, we truncated our analysis at 4 Gyr.

E. WHAT IF WE ONLY CONSIDERED MCQUILLAN'S PERIODS?

We argued in Section 2.1 that adopting the periods from Santos et al. (2019, 2021) yielded the best possible balance between homogeneity and sensitivity for both KOIs and for the broader Kepler sample. Nonetheless, it is interesting to consider what would happen if we were to analyze only the rotation periods from McQuillan et al. (2014). Figures 10 and 11 repeat the analysis, but make this alternate choice. Figure 10 shows that while the overall contours of the $P_{\rm rot}$ vs. $T_{\rm eff}$ distributions are similar, the Santos et al. distribution includes more stars, particularly at longer rotation periods. This is connected to a stronger noise-dependent cutoff in the McQuillan et al. (2014) sample than in the Santos et al. samples (see Masuda 2022b Figures 10 and 15). Figure 11 shows the impact on the inferred rotation-based age histograms: while the Santos et al. distribution peaks at 2.8-3.0 Gyr, the McQuillan et al. distribution peaks at 2.4-2.6 Gyr. A number of metrics shift. For instance, the ratio of the star formation rate 3 Gyr age to today is 2.81 ± 0.12 assuming the Santos et al. periods, and 2.24 ± 0.11 assuming the McQuillan et al. periods. Similarly, the ratio of "old" (2-3 Gyr) to "young" (0-1 Gyr) stars shifts from 2.1 in the Santos et al. case to 1.9 in the McQuillan et al. case. The K dwarf age distributions (Figure 11 lower panel) however appear quite similar. Generally, these plots support the conclusion that the $t_{\rm gyro}$ age distribution in the Kepler field is non-uniform, with a peak in the 2.3-3 Gyr range. Nonetheless, some of the details do shift depending on the choice of rotation detection pipeline.

This analysis is particularly interesting in relation to the question of how fast stars $\gtrsim$4 Gyr old spin down. If we lived in a universe in which stellar rotation rates and spot-induced photometric amplitudes remained *constant* after $\approx$3 Gyr, then older stars could contaminate the 2.3-3 Gyr peaks in Figures 6 and 11. This scenario deserves consideration, given *i)* asteroseismic evidence for slowed spin-down rates after $\approx$4 Gyr for Sun-like stars (e.g. van Saders et al. 2016; Saunders et al. 2024), and *ii)* the observation of a "long-period edge" in the $P_{\rm rot}$-$T_{\rm eff}$ distribution which may pile up over similar timescales (David et al. 2022). However, this pileup is thought to happen at $>$5 Gyr for late-G dwarfs and early K dwarfs (see Figure 4 by Saunders et al. 2024). This means that it cannot affect the 2.3 Gyr peak in the age distribution that we see for 4400-5400 K stars. Moreover, while some contamination by older stars may be present in the peaks, the analysis by Masuda (2022a) fitted isochrones to a high-quality subset of Kepler data, and found that the McQuillan et al. sample does not include many stars older than $\approx$ 4 Gyr. These lines of evidence suggest that the peak in the age distribution is not caused by a pile-up of much older stars with especially lethargic spin-down rates, but that it could be contaminated by them, especially for stars hotter than the Sun.

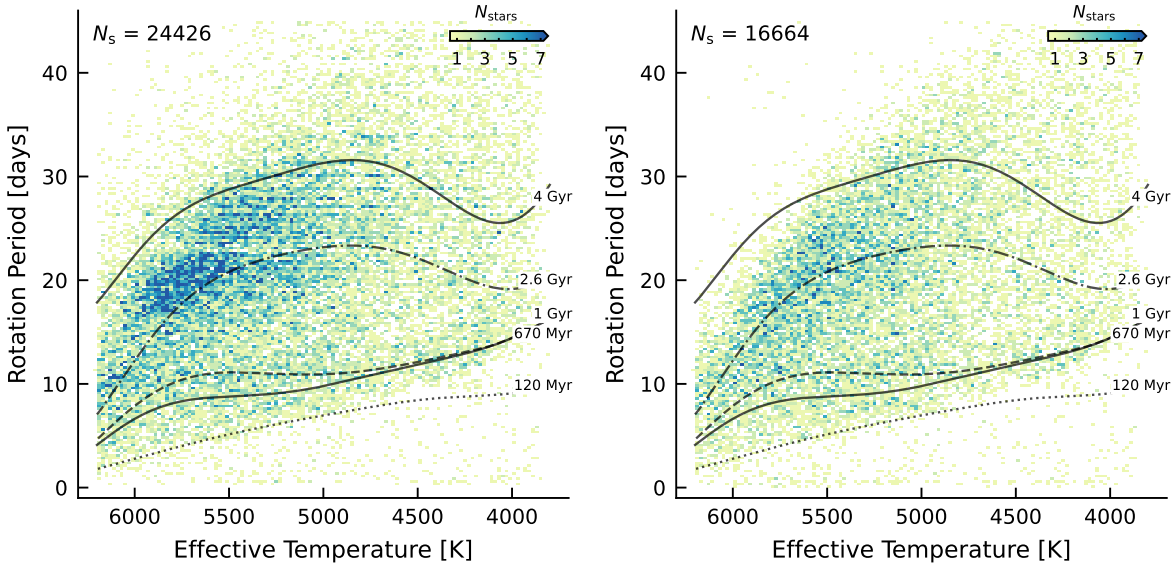

Figure 10. Variant of Figure 2, comparing the default rotation periods (*left*) from Santos et al. (2019, 2021) against the McQuillan et al. (2014) rotation periods (*right*). All stars are required to be amenable to rotation-based age dating (i.e. none of bit flags zero through ten raised).

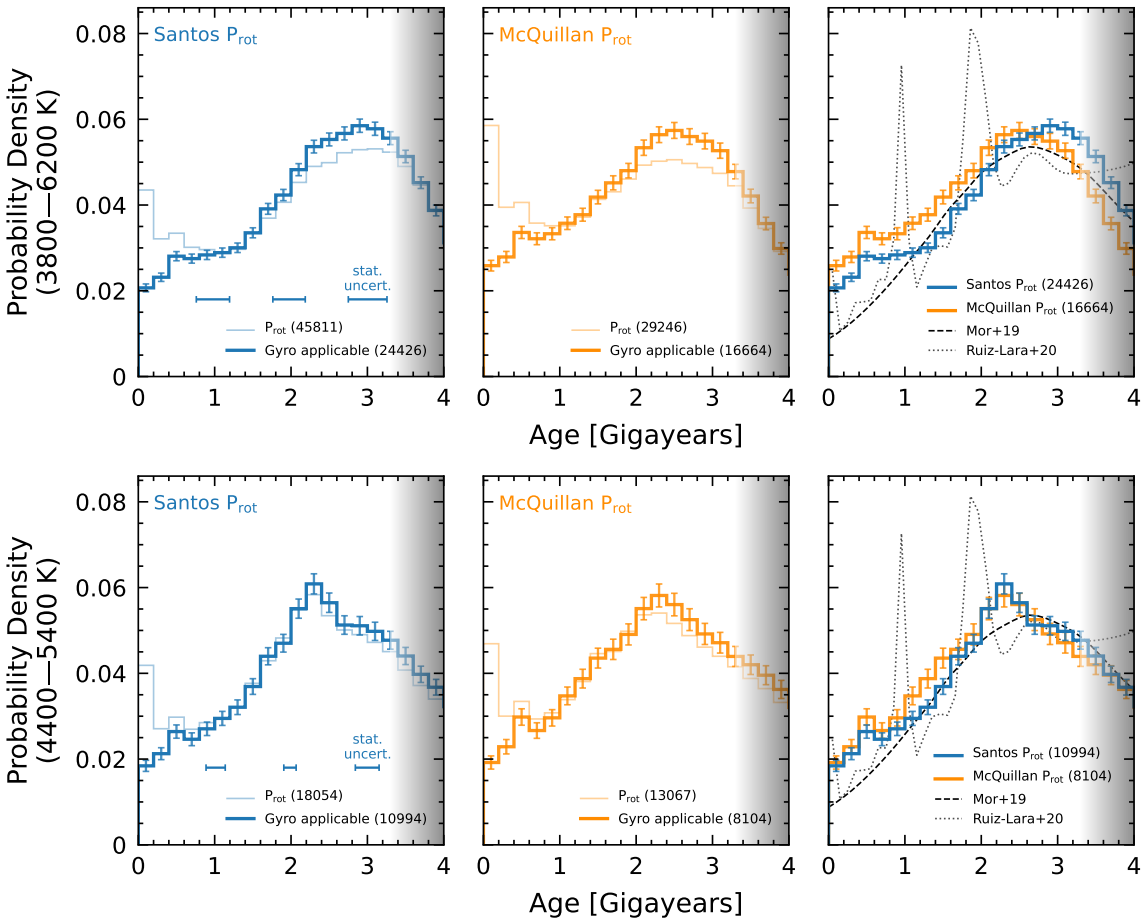

Figure 11. Variant of Figure 6, comparing our default adopted catalog of Santos et al. (2019, 2021) rotation periods against the rotation periods reported by McQuillan et al. (2014).